Nonlinear Dyn (2017) 90:2599–2626
DOI 10.1007/s11071-017-3826-1

ORIGINAL PAPER

Dynamics-based nonsingular interval model and luffing angular response field analysis of the DACS with narrowly bounded uncertainty

Bin Zhou · Bin Zi · Sen Qian

Received: 28 January 2017 / Accepted: 20 September 2017 / Published online: 5 October 2017

Abstract This paper develops a dynamics-based nonsingular interval model and proposes a first-order composite function interval perturbation method (FCFIPM) for luffing angular response field analysis of the dual automobile cranes system (DACS) with narrowly bounded uncertainty. By using the nonsingular interval model to describe a structure parameter with bounded uncertainty, the reasonable lower and upper bounds can be obtained, which is quite different from the traditional interval model with approximate bounds only from a large number of samples. Firstly, for the DACS with deterministic information, the inverse kinematics is analyzed, and the dynamic model of the DACS is established based on the virtual work principle and the inverse kinematics. Secondly, considering the nonsingularity of the dynamic response curves, a dynamics-based nonsingular interval model is introduced. Based on the nonsingular interval model, the interval luffing angular response vector equilibrium equation of the DACS is established. Thirdly, a first-order composite function interval perturbation method is proposed. In the FCFIPM, the composite function vectors are expanded by using the first-order Taylor series expansion, based on the differential property of composite function and monotonic analysis technique, the lower and upper bounds of the interval luffing angular response vector of the crane 1 and crane 2 of the DACS are determined. The first case is to investigate the deterministic kinematics and dynamics of the DACS with a given trajectory. The second case is provided to illustrate the detailed implementation process of constructing a dynamics-based nonsingular interval model. Finally, some numerical examples are given to verify the feasibility and efficiency of the FCFIPM for solving the luffing angular response field problem with narrowly interval parameters.

Keywords Dual automobile cranes system · Dynamics · Nonsingular interval model · Interval luffing angular response field · First-order composite function interval perturbation method

B. Zhou · B. Zi (✉) · S. Qian
School of Mechanical Engineering, Hefei University of Technology, 193 Tunxi road, Hefei 230009, China
e-mail: binzi.cumt@163.com

List of symbols

D	The length of A_1A_2
d	The length of payload C_1C_2
L_i	The length of lifting arm A_iB_i
γ_i	The luffing angular of lifting arm A_iB_i
$\boldsymbol{r}_{A_i}$	The position vector of joint point A_i in the base frame $\{B\}$
$\dot{\boldsymbol{r}}_{A_i}$	The velocity vector of joint point A_i
$\boldsymbol{r}_{B_i}$	The position vector of joint point B_i in the base frame $\{B\}$
$\dot{\boldsymbol{r}}_{B_i}$	The velocity vector of joint point B_i
$\boldsymbol{a}_{B_i}$	The acceleration vector of joint point B_i

$\boldsymbol{r}_{C_i}$	The position vector of joint point C_i in the base frame $\{B\}$
$\dot{\boldsymbol{r}}_{C_i}$	The velocity vector of joint point C_i
$\boldsymbol{a}_{C_i}$	The acceleration vector of joint point C_i
$\boldsymbol{r}_{O_i}$	The position vector of centroid O_i of lifting arm A_iB_i in the base frame $\{B\}$
$\boldsymbol{a}_{O_i}$	The acceleration of centroid O_i of lifting arm A_iB_i
$\boldsymbol{r}_{O_p}$	The position vector of centroid O_p in the base frame $\{B\}$
$\boldsymbol{v}_{O_p}$	The velocity vector of the origin O_p
$\boldsymbol{a}_{O_p}$	The acceleration vector of centroid O_p
$\boldsymbol{r}_{C_i}^{p}$	The position vector of joint point C_i in the moving frame $\{P\}$
$\boldsymbol{J}_{\boldsymbol{w}_{A_iB_i}}$	The partial angular velocity matrix of lifting arm A_iB_i
$\boldsymbol{J}_{\boldsymbol{v}_{B_i}}$	The partial velocity matrix of joint point B_i
$\boldsymbol{J}_{\boldsymbol{w}_p}$	The partial angular velocity matrix of the payload
$\boldsymbol{J}_{\boldsymbol{v}_{C_i}}$	The partial velocity matrix of joint point C_i
S_i	The length of hoisting rope B_iC_i
β_i	The rotation angle of hoisting rope B_iC_i
$\dot{\beta}_i$	The angular velocity of hoisting rope B_iC_i with respect to the lifting arm A_iB_i
m_i	The mass of lifting arm A_iB_i
$\boldsymbol{R}$	The rotation matrix from moving frame $\{P\}$ to base frame $\{B\}$
$\boldsymbol{R}'$	The deviation of $\boldsymbol{R}$ with respect to time
$\boldsymbol{R}''$	The deviation of $\boldsymbol{R}'$ with respect to time
θ	The rotation angle of $\{P\}$ relative to $\{B\}$
$\dot{\theta}$	The deviation of θ with respect to time
$\ddot{\theta}$	The deviation of $\dot{\theta}$ with respect to time
y	The Cartesian coordinates of the origin O_p along the y-axis.
z	The Cartesian coordinates of the origin O_p along the z-axis.
$\boldsymbol{F}_{A_iB_i}$	The inertia force of lifting arm A_iB_i respecting to joint point A_i
$\boldsymbol{M}_{A_iB_i}$	The inertia moment of lifting arm A_iB_i respecting to joint point A_i
$\boldsymbol{F}_p$	The inertia force of payload respecting to point C_1
$\boldsymbol{M}_p$	The inertia moment of payload respecting to point C_1
$\boldsymbol{\tau}$	The driving torque vector of the DACS
$\boldsymbol{\tau}_1$	The driving torque that impose on lifting arm A_1B_1
$\boldsymbol{\tau}_2$	The driving torque that impose on lifting arm A_2B_2
$\boldsymbol{J}_{\mathrm{DACS}}$	The kinematic Jacobian matrix of the DACS
$\boldsymbol{J}$	The dynamic Jacobian matrix of the DACS
$\boldsymbol{S}_i$	The matrix of the ith crane
$\boldsymbol{T}_i$	The vector of the ith crane
$\boldsymbol{\gamma}$	The luffing angular response vector.
$\boldsymbol{y}$	The interval parameter vector
y_r	The interval variable
$\boldsymbol{S}_i\ (\boldsymbol{K}_i\ (\boldsymbol{X}))$	The composite function matrix of the ith crane
$\boldsymbol{T}_i\ (\boldsymbol{K}_i\ (\boldsymbol{X}))$	The composite function vector of the ith crane
$\boldsymbol{y}^{\boldsymbol{c}}$	The midpoint value of the interval parameter vector $\boldsymbol{y}$
y_r^c	The midpoint value of interval parameter y_r
Δy_r	The interval radius of interval parameter y_r
$\boldsymbol{S}_i^c$	The midpoint value of composite function vector $\boldsymbol{S}_i\ (\boldsymbol{K}_i\ (\boldsymbol{y}))$
$\Delta_1\boldsymbol{S}_i^I$	The deviation interval of composite function vector $\boldsymbol{S}_i\ (\boldsymbol{K}_i\ (\boldsymbol{y}))$
$\boldsymbol{T}_i^c$	The midpoint value of composite function vector $\boldsymbol{T}_i\ (\boldsymbol{K}_i\ (\boldsymbol{y}))$
$\Delta_1\boldsymbol{T}_i^I$	The deviation interval of composite function vector $\boldsymbol{T}_i\ (\boldsymbol{K}_i\ (\boldsymbol{y}))$
$\boldsymbol{\gamma}_i^c$	The midpoint value of interval luffing angular response vector $\boldsymbol{\gamma}_i^I$
$\Delta_1\boldsymbol{\gamma}_i^I$	The deviation interval of interval luffing angular response vector $\boldsymbol{\gamma}_i^I$
$\overline{\boldsymbol{\gamma}_i}$	The upper bound of interval luffing angular response vector $\boldsymbol{\gamma}_i^I$
$\underline{\boldsymbol{\gamma}_i}$	The lower bound of interval luffing angular response vector $\boldsymbol{\gamma}_i^I$
D^c	The midpoint of length of A_1A_2
d^c	The midpoint of length of payload C_1C_2

L_1^c	The midpoint of length of lifting arm A_1B_1
L_2^c	The midpoint of length of lifting arm A_2B_2
ΔD	The interval radius of interval variable D
Δd	The interval radius of interval variable d
ΔL_1	The interval radius of interval variable L_1
ΔL_2	The interval radius of interval variable L_2
D_F	The interval change ratio of interval variable D
d_F	The interval change ratio of interval variable d
L_{1F}	The interval change ratio of interval variable L_1
L_{2F}	The interval change ratio of interval variable L_2

1 Introduction

During last decades, the dynamics and control of different kinds of cranes with different motions have been investigated widely [1], such as tower cranes [2,3], rotary cranes [4,5] and overhead cranes [6,7]. Recently, it is more popular to utilize multiple cranes to generate more hard operations in some modern construction projects. For example, Leban et al. [8] employed the Newton–Euler equations to construct the dynamic model of dual shipboard cranes system and an inverse kinematic control strategy for the underdetermined kinematic problem was presented, as shown in Fig. 1. Based on the Lagrange equation and D'Alembert principle, respectively, the dynamic model and error model of cooperative cable parallel manipulators for different multiple mobile cranes (CPMMC) were established by Zi et al. [9–11]. However, to narrow the gap between the numerical method and the actual situation, parametric uncertainties should be taken into consideration in practice to tackle the complicated problem for cranes [12,13].

Notably, research on uncertain technique has undergone rapid development in most practical engineering problems. This investigation has attracted an increasing amount of attention, especially in mechanical [14–16], thermal [17–19], acoustic [20–23] and civil engineering [24,25]. However, in traditional dynamic response analysis of automobile crane models, system parameters are rarely considered as uncertain parameters. Actually, uncertainty of structure parameters of an automobile crane may be resulted from the effects of external and inner factors [26], such as mechanical tolerances (e.g., designing/manufacturing/assembling errors, etc.), unpredictable external excitations (e.g., vibration motion, sea wave, etc.) [27], complicated environment factors (e.g., temperature level, wind load, etc.) [28] and so on. Generally speaking, the deterministic methods can only obtain an approximate solution of the practical response due to uncertainties in structure parameters [29,30]. Therefore, it is rather necessary to analyze the luffing angular response field problem of the dual automobile cranes system (DACS) with bounded uncertainty in structure parameters, as shown in Fig. 2 [31].

Up to now, the luffing angular response field problem of the DACS with interval parameters has not been researched yet. As a powerful approach, interval methods are widely used in many fields with quantifying

Fig. 1 Dual shipboard cranes system

Fig. 2 Dual automobile cranes system

uncertainties when information about the lower and upper bounds of some interval parameters is available [32]. Based on the perturbation theory and monotonic technique, the general idea of the interval methods is to compute the upper and lower bounds of response of systems or structures with interval parameters. In these methods, the Monte Carlo method (MCM) is the simplest method for uncertain response field problem [33–35]. Only if there exists a large number of samples, the accuracy of MCM can be guaranteed. In other words, with the increase in the number of samples, the accuracy of the response intervals obtained by the MCM will converge to theoretical intervals gradually; however, the computational cost increases accordingly. Thus, it is not appropriate for the MCM to be directly applied in large-scale engineering problems, but it can still be used as a reference method so as to compare the results with other interval methods. In order to decrease the computational time, based on first-order interval parameter perturbation method and the surface rail generation method, Wang et al. proposed a modified interval parameter perturbation method (MIPPM) to estimate response intervals in steady-state heat convection–diffusion problem and exterior acoustic field prediction [36,37]. Based on the interval analysis and Sherman–Morrison–Woodbury formula, a modified interval perturbation finite element method (MIPFEM) was proposed by Xia and Yu [38]. In this method, the interval matrix and the interval vector were expanded by using the first-order Taylor series, and the inverse interval matrix was approximated by using the first-order Neumann series. Besides, for an uncertain system with different kinds of interval parameters, such as a large uncertain interval variable or an interval random variable, Xia et al. [39] proposed different interval perturbation methods to handle these problems. Based on the so-called improved interval analysis (IIA) and rational series expansion (RSE), Muscolino et al. derived approximate explicit expressions of the frequency response function (FRF) matrix of linear discretized structures with uncertain parameters [40–43]. Recently, a Chebyshev interval method was proposed for solving differential equation systems with interval uncertainty. Besides, Chebyshev sampling methods (Chebyshev tensor product sampling method and Chebyshev collocation method)-based methodology was proposed for solving dynamic problem of rigid–flexible multibody systems with a large number of uncertain interval parameters [44,45].

As mentioned above, research on the dynamics of the DACS is still in its preliminary stage and has not been applied to the luffing angular response field problem with interval parameters yet. Firstly, how to construct a reasonable interval model, rather than simply applying a given interval model through a large variety of samples, has not solved. Secondly, the interval model compositing of uncertain structure parameters has not been applied in the prediction of luffing angular response field of the DACS with bounded uncertainty, in other words, researchers have not developed an equilibrium response equation of the DACS with interval parameters yet. Thirdly, the application of interval methods in the luffing angular response field problem of the DACS with composite functions, especially for the prediction of the interval luffing angular response field with narrow uncertainty, has not explored yet.

In this paper, a first-order composite function interval perturbation method (FCFIPM) is proposed for the prediction of the luffing angular response field of the DACS with narrowly interval parameters. The main procedures of the interval response field prediction are divided into three steps. The first step is to construct the kinematics and dynamics of the DACS with deterministic information. Based on the dynamic response model and the nonsingularity of the response curves, a dynamics-based nonsingular interval model is constructed to obtain reasonable bounds of all the interval variables in the second step. Subsequently, the luffing angular equilibrium equation of the DACS with interval parameters is derived. Based on the first-order Taylor series expansions, the differential property of composite function and monotonic analysis technique, the first-order composite function interval perturbation method (FCFIPM) for the luffing angular response field prediction of the DACS with narrowly bounded uncertainty is proposed in the third step. Finally, examples and results are presented and discussed as well.

The remainder of this paper is organized as follows. In Sect. 2, the kinematics of the DACS is analyzed by the inverse kinematic method. Based on the virtual work principle and the kinematics, the dynamic model of the DACS is derived in Sect. 3. In Sect. 4, a dynamics-based nonsingular interval model is constructed, based on the above interval model, the DACS equilibrium equation with the nonsingular interval model is generated. In Sect. 5, based on the differential property of composite function, the first-order Taylor series expansion and the first-order Neumann series, a first-order

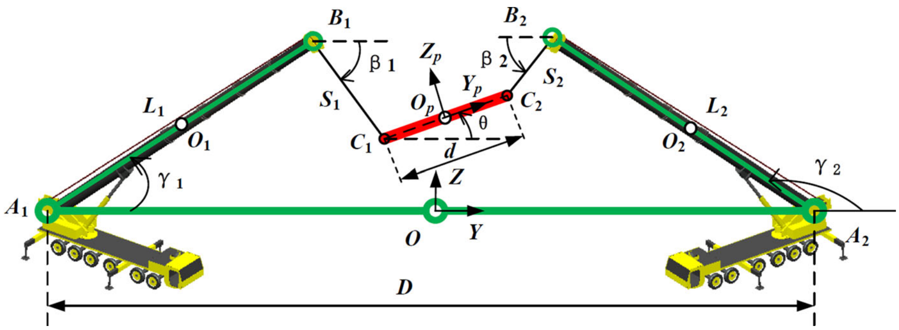

Fig. 3 2-D model of the DACS

composite function interval perturbation method for the interval luffing angular response field of the DACS with narrowly interval parameters is proposed. In Sect. 6, the first case is to provide some simulations under a given trajectory, in order to investigate the dynamics. The second case is performed to obtain the dynamics-based nonsingular interval model of the DACS. Based on the above dynamics-based nonsingular interval model, the third case is given for the verification of the effectiveness and feasibility of the first-order composite function interval perturbation method dealt with narrowly interval parameters. And the effect of different kinds of interval models on the DACS response field is also investigated in details. Finally, some concluding remarks are reported in Sect. 7.

2 Kinematics

2.1 Structural description

The dual automobile cranes system (DACS) is widely used in hoisting heavy payload applied in engineering operations. Considering the DACS model shown in Fig. 2, it is consisted of two automobile cranes and a payload. Each automobile crane includes one lifting arm, one luffing cylinder, one rotating table and one hoisting rope.

In this paper, we consider the luffing motions of two cranes, simultaneously. According to the work of Leban et al. [8], the whole system can make the payload moving in two-axis (Y and Z axes) translation and rotating around single axis perpendicular to the O-YZ plane.

For the DACS model, the following assumptions are made for simplicity [26,46]

1. The payload is symmetrical strictly, and the hoisting ropes are never slack.
2. Inertia forces of lifting arms and the payload are not neglected.
3. The masses of the hoisting ropes are considered to be neglected compared with other structures of the system.

Referring to Fig. 3, the base frame $\{B\} : O - YZ$ and the moving frame $\{P\} : O_p - Y_p Z_p$ are fixed on the centers of A_1A_2 and C_1C_2, respectively. The A_i, B_i and C_i $(i = 1, 2)$ denote the three key joint points of the ith crane, where A_i denotes the hinge point of the lifting arm A_iB_i and the ith rotating table, B_i denotes the hinge point of the lifting arm A_iB_i and the hoisting rope B_iC_i, C_i denotes the hinge point of the hoisting rope B_iC_i and the payload C_1C_2. The length of the lifting arm A_iB_i is L_i. The length of the hoisting rope B_iC_i is S_i. The lengths of A_1A_2 and C_1C_2 are D and d, respectively. The luffing angle of the lifting arms A_iB_i is γ_i. The y, z and θ are the three Cartesian coordinates of the origin O_p.

2.2 Inverse kinematics

In this section, based on the inverse kinematics, the goal of this subsection is to establish the relationship function between system variables (D, d, L_i, y, z and θ) and response variables (γ_i).

The position vectors of joint points A_i (A_1 and A_2) in the base frame $\{B\}$ can be expressed as

$$\boldsymbol{r}_{A_i} = \frac{1}{2}\left[(-1)^i\, D \quad 0\right]^{\mathrm{T}} \tag{1}$$

The position vectors of joint points B_i (B_1 and B_2) in the base frame $\{B\}$ can be expressed as

$$\boldsymbol{r}_{B_i} = \boldsymbol{r}_{A_i} + L_i \begin{bmatrix} \cos\gamma_i \\ \sin\gamma_i \end{bmatrix}, \quad i = 1, 2 \tag{2}$$

The position vector of joint points C_i in the moving frame $\{P\}$ can be expressed as

$$\boldsymbol{r}_{C_i}^{p} = \frac{1}{2}\left[(-1)^i d \quad 0\right]^{\mathrm{T}} \tag{3}$$

The position vector of joint point C_i in the base frame $\{B\}$ can be expressed as

$$\boldsymbol{r}_{C_i} = \boldsymbol{r}_{O_p} + \boldsymbol{R}\cdot\boldsymbol{r}_{C_i}^{p},\ i = 1, 2 \tag{4}$$

where $\boldsymbol{r}_{O_p}$ is the position vector of centroid O_p in the base frame $\{B\}$, and $\boldsymbol{r}_{O_p} = (y\ z)^T$. $\boldsymbol{R}$ denotes the rotation matrix from moving frame $\{P\}$ to base frame $\{B\}$, and $\boldsymbol{R} = \begin{bmatrix} \cos\theta & -\sin\theta \\ \sin\theta & \cos\theta \end{bmatrix}$.

The constraint equation associated with the ith hoisting rope can be expressed as

$$\left\|\boldsymbol{r}_{C_i} - \boldsymbol{r}_{B_i}\right\| = S_i, \quad i = 1, 2 \tag{5}$$

Substituting Eqs. (2)–(4) into (5), the above constraint equation can be expressed as

$$\begin{cases} \left(y - \frac{d\cos\theta}{2} + \frac{D}{2} - L_1\cos\gamma_1\right)^2 + \left(z - \frac{d\sin\theta}{2} - L_1\sin\gamma_1\right)^2 = S_1^2 \\ \left(y + \frac{d\cos\theta}{2} - \frac{D}{2} - L_2\cos\gamma_2\right)^2 + \left(z + \frac{d\sin\theta}{2} - L_2\sin\gamma_2\right)^2 = S_2^2 \end{cases} \tag{6}$$

Equation (6) can be rewritten as

$$K_{1i}\sin\gamma_i + K_{2i}\cos\gamma_i + K_{3i} = 0, \quad i = 1, 2 \tag{7}$$

where

$$K_{11} = -2L_1\left(z - \frac{d\sin\theta}{2}\right),$$
$$K_{21} = -2L_1\left(y - \frac{d\cos\theta}{2} + \frac{D}{2}\right),$$
$$K_{31} = \left(y - \frac{d\cos\theta}{2} + \frac{D}{2}\right)^2 + \left(z - \frac{d\sin\theta}{2}\right)^2 + L_1^2 - S_1^2,$$
$$K_{12} = -2L_2\left(z + \frac{d\sin\theta}{2}\right),$$
$$K_{22} = -2L_2\left(y + \frac{d\cos\theta}{2} - \frac{D}{2}\right),$$
$$K_{32} = \left(y + \frac{d\cos\theta}{2} - \frac{D}{2}\right)^2 + \left(z + \frac{d\sin\theta}{2}\right)^2 + L_2^2 - S_2^2. \tag{8}$$

Based on Eq. (7), the inverse kinematic solution for the DACS can be expressed as

$$\gamma_i = 2\tan^{-1}\frac{-K_{1i} \pm \sqrt{K_{1i}^2 + K_{2i}^2 - K_{3i}^2}}{K_{3i} - K_{2i}}, \quad i = 1, 2 \tag{9}$$

2.3 Jacobian matrix

Jacobian matrix is a velocity mapping from input actuators to payload. In this subsection, it is used to obtain the velocity and acceleration of joints in the luffing motion of the DACS.

Taking the time derivative of Eq. (7) obtains

$$K_{1i}\cos\gamma_i\cdot\dot{\gamma}_i + \sin\gamma_i\cdot\dot{K}_{1i} - K_{2i}\sin\gamma_i\cdot\dot{\gamma}_i + \cos\gamma_i\cdot\dot{K}_{2i} + \dot{K}_{3i} = 0, \quad i = 1, 2 \tag{10}$$

Equation (10) can be rewritten as

$$\begin{bmatrix} M_{11} & 0 \\ 0 & M_{22} \end{bmatrix}\begin{bmatrix} \dot{\gamma}_1 \\ \dot{\gamma}_2 \end{bmatrix} = \begin{bmatrix} N_{11} & N_{12} & N_{13} \\ N_{21} & N_{22} & N_{23} \end{bmatrix}\begin{bmatrix} \dot{y} \\ \dot{z} \\ \dot{\theta} \end{bmatrix} \tag{11}$$

where

$$M_{11} = K_{11}\cos\gamma_1 - K_{21}\sin\gamma_1,$$
$$M_{22} = K_{12}\cos\gamma_2 - K_{22}\sin\gamma_2,$$
$$N_{11} = -2L_1\cos\gamma_1 + 2\left(y - \frac{d\cos\theta}{2} + \frac{D}{2}\right),$$
$$N_{12} = -2L_1\sin\gamma_1 + 2\left(z - \frac{d\sin\theta}{2}\right),$$
$$N_{21} = -2L_2\cos\gamma_2 + 2\left(y + \frac{d\cos\theta}{2} - \frac{D}{2}\right),$$
$$N_{22} = -2L_2\sin\gamma_2 + 2\left(z + \frac{d\sin\theta}{2}\right),$$
$$N_{13} = \frac{d\sin\theta}{2}N_{11} - \frac{d\cos\theta}{2}$$
$$N_{12}, N_{23} = -\frac{d\sin\theta}{2}N_{21} + \frac{d\cos\theta}{2}N_{22}. \tag{12}$$

Let $\boldsymbol{M} = \begin{bmatrix} M_{11} & 0 \\ 0 & M_{22} \end{bmatrix}$ and $\boldsymbol{N} = \begin{bmatrix} N_{11} & N_{12} & N_{13} \\ N_{21} & N_{22} & N_{23} \end{bmatrix}$, $\boldsymbol{J}_{\text{DACS}}$ is defined as the kinematic Jacobian matrix of the DACS, which can be expressed as

$$\boldsymbol{J}_{\text{DACS}} = \boldsymbol{M}^{-1}\boldsymbol{N} \tag{13}$$

3 Dynamics

3.1 Partial velocity vector and partial angular velocity matrix

To establish the dynamic model of the DACS, in this subsection, the partial velocity vector and partial angular velocity matrix of every component of the system should be calculated firstly. The partial velocity vector of the component or joint point means the mapping relationship between the velocity of the centroid of payload and the component or joint point, and the partial angular velocity matrix of the component or joint point means the mapping relationship between the angular velocity of the centroid of payload and the component or joint point.

Taking the time derivative of Eqs. (2) and (5) obtains

$$\begin{aligned} \dot{\boldsymbol{r}}_{B_i} &= \dot{\boldsymbol{r}}_{A_i} + L_i\dot{\gamma}_i \begin{bmatrix} -\sin\gamma_i \\ \cos\gamma_i \end{bmatrix} \\ &= L_i\dot{\gamma}_i \begin{bmatrix} -\sin\gamma_i \\ \cos\gamma_i \end{bmatrix},\ i = 1,2 \end{aligned} \tag{14}$$

$$\begin{aligned} \dot{\boldsymbol{r}}_{C_i} &= \boldsymbol{v}_{O_p} + \boldsymbol{R}'\boldsymbol{r}_{C_i}^{p} \\ &= \dot{\boldsymbol{r}}_{B_i} + S_i\dot{\beta}_i \begin{bmatrix} -\sin\beta_i \\ \cos\beta_i \end{bmatrix},\ i = 1,2 \end{aligned} \tag{15}$$

where $\boldsymbol{v}_{O_p}$ is the velocity vector of the origin O_p, $\boldsymbol{v}_{O_p} = \begin{bmatrix} \dot{y} & \dot{z} \end{bmatrix}^{\mathrm{T}}$ and $\boldsymbol{R}'$ can be expressed as $\boldsymbol{R}' = \dot{\theta}\begin{bmatrix} -\sin\theta & -\cos\theta \\ \cos\theta & -\sin\theta \end{bmatrix}$.

Referring to the work of Zhu and Dou [47] and Wu et al. [48], based on Eq. (13), the partial angular velocity matrix of lifting arm A_iB_i can be expressed as

$$\boldsymbol{J}_{\boldsymbol{w}_{A_iB_i}} = \begin{bmatrix} \frac{N_{i1}}{M_{ii}} & \frac{N_{i2}}{M_{ii}} & \frac{N_{i3}}{M_{ii}} \end{bmatrix},\ i = 1,2 \tag{16}$$

Similarly, based on Eq. (14), the partial velocity matrix of joint point B_i can be expressed as

$$\boldsymbol{J}_{\boldsymbol{v}_{B_i}} = \begin{bmatrix} -L_i\sin\gamma_i\cdot\frac{N_{i1}}{M_{ii}} & -L_i\sin\gamma_i\cdot\frac{N_{i2}}{M_{ii}} & -L_i\sin\gamma_i\cdot\frac{N_{i3}}{M_{ii}} \\ L_i\cos\gamma_i\cdot\frac{N_{i1}}{M_{ii}} & L_i\cos\gamma_i\cdot\frac{N_{i2}}{M_{ii}} & L_i\cos\gamma_i\cdot\frac{N_{i3}}{M_{ii}} \end{bmatrix},\ i = 1,2 \tag{17}$$

In order to simplify the derivation, here we assume that lifting arms A_iB_i $(i = 1,2)$ are both symmetrical. Thus, the partial velocity matrix of lifting arm A_iB_i can be expressed as

$$\boldsymbol{J}_{\boldsymbol{v}_{A_iB_i}} = \frac{1}{2}\boldsymbol{J}_{\boldsymbol{v}_{B_i}},\ i = 1,2 \tag{18}$$

Similarly, based on Eq. (15), the partial angular velocity matrix of the payload and partial velocity matrix of joint points C_i can be expressed as

$$\boldsymbol{J}_{\boldsymbol{w}_p} = \begin{bmatrix} 1 & 0 & 0 \end{bmatrix} \tag{19}$$

$$\boldsymbol{J}_{\boldsymbol{v}_{C_i}} = \begin{bmatrix} -(-1)^i\,\frac{\sin\theta}{2}d & 1 & 0 \\ -(-1)^i\,\frac{\cos\theta}{2}d & 0 & 1 \end{bmatrix},\ i = 1,2 \tag{20}$$

3.2 Acceleration matrix

In this subsection, in order to describe the inertia force and moment of lifting arms and payload, the acceleration vectors of joint points and the acceleration matrix of the system should be analyzed.

By taking the time derivative of Eqs. (14) and (15), the acceleration vectors of joint points B_i and C_i can be expressed as

$$\boldsymbol{a}_{B_i} = L_i\ddot{\gamma}_i \begin{bmatrix} -\sin\gamma_i \\ \cos\gamma_i \end{bmatrix} - L_i\dot{\gamma}_i^2 \begin{bmatrix} \cos\gamma_i \\ \sin\gamma_i \end{bmatrix},\ i = 1,2 \tag{21}$$

$$\boldsymbol{a}_{C_i} = \boldsymbol{a}_{O_p} + \boldsymbol{R}''\cdot\boldsymbol{r}_{C_i}^{p},\ i = 1,2 \tag{22}$$

where $\boldsymbol{a}_{O_p}$ is the acceleration vector of centroid O_p, and $\boldsymbol{R}''$ can be expressed as

$$\boldsymbol{R}'' = \ddot{\theta}\begin{bmatrix} -\sin\theta & -\cos\theta \\ \cos\theta & -\sin\theta \end{bmatrix} + \dot{\theta}^2\begin{bmatrix} -\cos\theta & \sin\theta \\ -\sin\theta & -\cos\theta \end{bmatrix} \tag{23}$$

Similarly, based on Eq. (21), the acceleration vector of centroid O_i of lifting arm A_iB_i can be expressed as

$$\boldsymbol{a}_{O_i} = \frac{L_i}{2}\ddot{\gamma}_i \begin{bmatrix} -\sin\gamma_i \\ \cos\gamma_i \end{bmatrix} - \frac{L_i}{2}\dot{\gamma}_i^2 \begin{bmatrix} \cos\gamma_i \\ \sin\gamma_i \end{bmatrix},\ i = 1,2 \tag{24}$$

3.3 Inertia force and moment

Based on the analysis in Sect. 3.2, the goal of this subsection is to obtain the inertia force and moment of lifting arms and payload, respectively.

Considering the joint point A_i is fixed, the inertia force and moment of lifting arm A_iB_i respecting to joint point A_i can be expressed as

$$\boldsymbol{F}_{A_iB_i} = -m_i\left(\boldsymbol{a}_{A_i} + \boldsymbol{a}_{O_i}\right) = -m_i\boldsymbol{a}_{O_i},\ i = 1, 2 \quad (25)$$

$$\begin{aligned}\boldsymbol{M}_{A_iB_i} &= -\ddot{\gamma}_i I_i - m_i\frac{L_i}{2}\left[-\sin\gamma_i\ \cos\gamma_i\right]\boldsymbol{a}_{A_i}\\ &= -\ddot{\gamma}_i I_i,\ i = 1, 2\end{aligned} \quad (26)$$

where m_i is the mass of lifting arm A_iB_i, I_i is the moment of inertia of lifting arm A_iB_i respecting to its centroid, and $I_i = \frac{m_iL_i^2}{3}$.

The inertia force and moment of payload respecting to point C_1 can be expressed as

$$\boldsymbol{F}_p = -m_p\boldsymbol{a}_{C_1} \quad (27)$$

$$\boldsymbol{M}_p = -\ddot{\theta}I_p - m_p\frac{d}{2}\left[-\sin i\ \cos i\right]\boldsymbol{a}_{O_p} \quad (28)$$

where m_p is the mass of payload, I_p is the moment of inertia of payload respecting to joint point C_1, and $I_p = \frac{m_pd^2}{3}$.

In this paper, it is noted that the inertia force and moment of hoisting ropes are thought as zero for their masses are neglected.

3.4 Dynamic modeling

Based on the virtual work principle, combining Eqs. (13), (16), (18)–(20) and (25)–(28), the dynamic model of the DACS can be expressed as follows

$$\boldsymbol{J}_{\mathrm{DACS}}^{\mathrm{T}}\boldsymbol{\tau} + \left\{\sum_{i=1}^{2}\left[\left(\boldsymbol{F}_{A_iB_i} + m_i\mathbf{g}\right)^{\mathrm{T}}\ \left(\boldsymbol{M}_{A_iB_i}\right)^{\mathrm{T}}\right]\begin{bmatrix}\boldsymbol{J}_{\boldsymbol{v}_{A_iB_i}}\\ \boldsymbol{J}_{\boldsymbol{w}_{A_iB_i}}\end{bmatrix} + \left[\left(\boldsymbol{F}_p + m_p\mathbf{g}\right)^{\mathrm{T}}\ \left(\boldsymbol{M}_p\right)^{\mathrm{T}}\right]\begin{bmatrix}\boldsymbol{J}_{\boldsymbol{v}_{C_1}}\\ \boldsymbol{J}_{\boldsymbol{w}_p}\end{bmatrix}\right\}^{\mathrm{T}} = \mathbf{0},\ i = 1, 2 \quad (29)$$

where driving torque vector of the DACS is denoted as $\boldsymbol{\tau} = \left[\boldsymbol{\tau}_1\ \boldsymbol{\tau}_2\right]^{\mathrm{T}}$, where $\boldsymbol{\tau}_1$ and $\boldsymbol{\tau}_2$ are the driving torques that impose on lifting arms A_1B_1 and A_2B_2, respectively.

From Eq. (29), the driving torque vector of the DMCS can be expressed as

$$\boldsymbol{\tau} = -\left(\boldsymbol{J}_{\mathrm{DACS}}^{\mathrm{T}}\right)^{-1}\left\{\sum_{i=1}^{2}\left[\left(\boldsymbol{F}_{A_iB_i}+m_i\mathbf{g}\right)^{\mathrm{T}}\ \left(\boldsymbol{M}_{A_iB_i}\right)^{\mathrm{T}}\right] \times\begin{bmatrix}\boldsymbol{J}_{\boldsymbol{v}_{A_iB_i}}\\ \boldsymbol{J}_{\boldsymbol{w}_{A_iB_i}}\end{bmatrix} + \left[\left(\boldsymbol{F}_p+m_p\mathbf{g}\right)^{\mathrm{T}}\ \left(\boldsymbol{M}_p\right)^{\mathrm{T}}\right]\begin{bmatrix}\boldsymbol{J}_{\boldsymbol{v}_{C_1}}\\ \boldsymbol{J}_{\boldsymbol{w}_p}\end{bmatrix}\right\}^{\mathrm{T}} \quad (30)$$

The main objective of the inverse dynamic model of the DACS is to determine the driving torque $\boldsymbol{\tau}_i$ $(i = 1, 2)$ of each automobile crane when kinematic Jacobian matrix $\boldsymbol{J}_{\mathrm{DACS}}$, partial velocity of joint points A_i and C_1, partial angular velocity matrices and acceleration matrices of lifting arm A_iB_i and payload C_1C_2 are given.

4 Luffing angular response field problem with bounded uncertainty

4.1 Definition of dynamics-based nonsingular interval model

According to the work of Jiang et al. [49], a dynamics-based nonsingular interval model is proposed to obtain a reasonable interval parameters set, which can make distribution curve of dynamic response of the DACS smooth without any saltation.

Without loss of generation, let the continuous interval variable $\boldsymbol{f}\left(\boldsymbol{Y}^{\boldsymbol{I}}, t\right)$ denote the dynamic response function of multiple interval variables which are represented by the interval vector $\boldsymbol{Y}^{\boldsymbol{I}} = \left(y_1^{\mathrm{I}}, \ldots, y_r^{\mathrm{I}}, \ldots, y_n^{\mathrm{I}}\right)$. For simplicity, all interval variables are assumed to be independent of each other with small uncertainty. According to the first-order Taylor series expansion and the perturbation theory, the dynamic response function $\boldsymbol{f}\left(\boldsymbol{Y}^{\boldsymbol{I}}, t\right)$ can be expressed as

$$\boldsymbol{f}\left(\boldsymbol{Y}^{\boldsymbol{I}}, t\right) = f\left(\boldsymbol{Y}^{\boldsymbol{c}}, t\right) + \sum_{i=1}^{n}\left\{\left.\frac{\partial\boldsymbol{f}\left(\boldsymbol{Y}^{\boldsymbol{I}}, t\right)}{\partial y_i^{\mathrm{I}}}\right|_{\boldsymbol{Y}^{\boldsymbol{c}}}\right\}\left(y_r - y_r^{\mathrm{c}}\right) + R \quad (31)$$

where R is the remainder term.

In complicated engineering problems, the deviation of $\boldsymbol{f}\left(\boldsymbol{Y}^{\boldsymbol{I}}, t\right)$ with respect to the time t, i.e., $\frac{\partial\boldsymbol{f}\left(\boldsymbol{Y}^{\boldsymbol{I}}, t\right)}{\partial t}$ can't be obtained in some stochastic points from the interval of y_i^{I}, in other words, some unreasonable samples of uncertain variables can result in singular matrix [50].

In this case, in order to obtain the reasonable bound for every interval parameter, based on the dynamic response function $\boldsymbol{f}\left(\boldsymbol{Y}^{\boldsymbol{I}}, t\right)$ in Eq. (31), a dynamics-based nonsingular interval model can be defined as

$$
\begin{aligned}
&\text{Find } y_r \epsilon y_r^{\mathrm{I}}=\left[\underline{y_r}, \overline{y_r}\right] \\
&\text{s.t. } \nexists \frac{\partial f\left(y_1^{\mathrm{c}}, \ldots, \underline{y_r}-\sigma, \ldots, y_n^{\mathrm{c}}, t\right)}{\partial t} \text{ and } \nexists \frac{\partial f\left(y_1^{\mathrm{c}}, \ldots, \overline{y_r}+\sigma, \ldots, y_n^{\mathrm{c}}, t\right)}{\partial t} \\
&\text{and } \exists \frac{\partial f\left(y_1^{\mathrm{c}}, \ldots, y_r, \ldots, y_n^{\mathrm{c}}, t\right)}{\partial t} \\
&\underline{y_r}<y_r<\overline{y_r}, \quad r=1, \cdots, n .
\end{aligned} \tag{32}
$$

where $\blacksquare^c$ is the symbol of midpoint value. σ is an infinitesimal. $\underline{y_r}$ and $\overline{y_r}$ are lower and upper bounds of the rth interval parameter vector y_r^{I}, respectively. n is the total number of interval parameters.

4.2 Luffing angular response equilibrium equation with nonsingularity

Due to the nonnegative of the luffing angular response γ_i $(i=1,2)$, Eq. (9) can also be written as

$$
\tan \frac{\gamma_i}{2}=\frac{\sqrt{K_{1i}^2+K_{2i}^2-K_{3i}^2}-K_{1i}}{K_{3i}-K_{2i}}, \quad i=1,2 \tag{33}
$$

To simplify the process of analyzing the luffing angular response equation of the DACS with interval parameters, we rewrite Eq. (33) as the following form

$$
\boldsymbol{S}_i=\boldsymbol{T}_i \boldsymbol{\gamma}_i, \quad i=1,2 \tag{34}
$$

where $\boldsymbol{S}_i$ and $\boldsymbol{T}_i$ are the matrix and vector of the ith crane; $\boldsymbol{\gamma}_i$ is the luffing angular response vector of the ith crane. They can be expressed as

$$
\begin{aligned}
&\boldsymbol{S}_i=\sqrt{K_{1i}^2+K_{2i}^2-K_{3i}^2}-K_{1i}, \\
&\boldsymbol{T}_i=K_{3i}-K_{2i}, \quad \boldsymbol{\gamma}_i=\tan \frac{\gamma_i}{2} .
\end{aligned} \tag{35}
$$

In actual crane engineering problems, due to the effects of production limitations and manufacturing errors, the uncertainty in structure parameters is unavoidable. Furthermore, according to the work of Zi and Zhou [26] and Gao et al. [27,30], the allowable ranges of an uncertain structure parameters usually belong to some interval. In this paper, the uncertainty of structure parameters can be quantitatively described as the interval parameters with small interval change ratios.

According to the definition of dynamics-based nonsingular interval model in Sect. 4.1, we assume that the allowable interval vector is composed of all the independent interval variables of the DACS with narrow uncertainty, in other words, a reasonable interval model is constructed, which can be defined as

$$
\boldsymbol{y} \in \boldsymbol{y}^I=\left(y_r^I\right)=[\underline{\boldsymbol{y}}, \overline{\boldsymbol{y}}], \; y_r \in y_r^I=\left(y_r^I\right)=\left[\underline{y_r}, \overline{y_r}\right] . \tag{36}
$$

where $\underline{\boldsymbol{y}}$ and $\overline{\boldsymbol{y}}$ are lower and upper bounds of interval parameter vector $\boldsymbol{y}$, respectively.

Therefore, the luffing angular response equilibrium equation (Eq. 34) of the DACS with nonsingularity can be rewritten as

$$
\boldsymbol{S}_i\left(\boldsymbol{K}_i(\boldsymbol{y})\right)=\boldsymbol{T}_i\left(\boldsymbol{K}_i(\boldsymbol{y})\right) \boldsymbol{\gamma}_i(\boldsymbol{y}), \quad i=1,2 \tag{37}
$$

where $\boldsymbol{S}_i\left(\boldsymbol{K}_i(\boldsymbol{y})\right)$ and $\boldsymbol{T}_i\left(\boldsymbol{K}_i(\boldsymbol{y})\right)$ are called the composite function matrix and the composite function vector of the ith crane respecting to interval parameter vector $\boldsymbol{y}$, respectively, which can be expressed in the following form

$$
\begin{aligned}
\boldsymbol{S}_i\left(\boldsymbol{K}_i(\boldsymbol{y})\right)= & \sqrt{K_{1i}(\boldsymbol{y})^2+K_{2i}(\boldsymbol{y})^2-K_{3i}(\boldsymbol{y})^2} \\
& -K_{1i}(\boldsymbol{y}), \\
\boldsymbol{T}_i\left(\boldsymbol{K}_i(\boldsymbol{y})\right)= & K_{3i}(\boldsymbol{y})-K_{2i}(\boldsymbol{y}) .
\end{aligned} \tag{38}
$$

Based on Eq. (36), $\boldsymbol{K}_i(\boldsymbol{y})$ stands for the membership function vector of interval parameter vector $\boldsymbol{y}$, which can be expressed as

$$
\boldsymbol{K}_i(\boldsymbol{y})=\left\{K_{1i}(\boldsymbol{y}), K_{2i}(\boldsymbol{y}), K_{3i}(\boldsymbol{y})\right\}^{\mathrm{T}} \tag{39}
$$

where $K_{1i}(\boldsymbol{y})$, $K_{2i}(\boldsymbol{y})$ and $K_{3i}(\boldsymbol{y})$ stand for three membership expressions of interval parameter vector $\boldsymbol{y}$, respectively.

Theoretical solution set of Eq. (37) is defined as

$$
\epsilon=\left\{\boldsymbol{\gamma}_i^I \mid \boldsymbol{S}_i\left(\boldsymbol{K}_i(\boldsymbol{y})\right)=\boldsymbol{T}_i\left(\boldsymbol{K}_i(\boldsymbol{y})\right) \boldsymbol{\gamma}_i(\boldsymbol{y}), \in \boldsymbol{y}^I\right\} \tag{40}
$$

In general, the theoretical solution set ϵ has a very complicated region. Therefore, it is rather hard to solve Eq. (40) directly. According to the work of Wang and Qiu [19,36,37] and Xia et al. [38,39], the appropriate solution of interval luffing angular response vector $\boldsymbol{\gamma}_i^I$ is usually transformed to solve the smallest closed interval which includes the theoretical solution set ϵ. The approximate solution can be expressed as

$$
\boldsymbol{\gamma}_i^I=\left[\underline{\boldsymbol{\gamma}_i}, \overline{\boldsymbol{\gamma}_i}\right] \tag{41}
$$

where $\underline{\boldsymbol{\gamma}_i}$ and $\overline{\boldsymbol{\gamma}_i}$ are the lower and upper bounds of the smallest closed interval, respectively.

Thus, Eq. (37) can be rewritten as

$$\boldsymbol{S}_i\left(\boldsymbol{K}_i\left(\boldsymbol{y}\right)\right) = \boldsymbol{T}_i\left(\boldsymbol{K}_i\left(\boldsymbol{y}\right)\right)\boldsymbol{\gamma}_i^I,\ i = 1, 2 \tag{42}$$

In this paper, we define interval luffing angular response field as the quantified effect of interval parameters on the luffing angular response vector of the DACS, which can be expressed as the bounds (lower and upper bound) of luffing angular response vector.

5 First-order composite function interval perturbation method (FCFIPM)

In this section, the interval luffing angular response field of the DACS with narrow uncertainty will be calculated by the proposed first-order composite function interval perturbation method (FCFIPM). As we know, for an uncertain system with bounded parameters, if the ranges of all the bounded parameters are all rather narrow, the accuracy and computational cost of applying the first-order Taylor series expansion for the nonlinear functions are acceptable [19,26,36,37,39].

Based on the differential property of composite function and neglecting the higher-order terms, the first-order Taylor expansions of composite function matrix $\boldsymbol{S}_i\left(\boldsymbol{K}_i\left(\boldsymbol{y}\right)\right)$ at the midpoints of the interval parameter vector $\boldsymbol{y}$ can be expressed as

$$\boldsymbol{S}_i\left(\boldsymbol{K}_i\left(\boldsymbol{y}\right)\right) = \boldsymbol{S}_i^c + \Delta_1\boldsymbol{S}_i^I \tag{43}$$

where $\boldsymbol{S}_i^c$ and $\Delta_1\boldsymbol{S}_i^I$ are the midpoint value and deviation interval of the composite function matrix $\boldsymbol{S}_i\left(\boldsymbol{K}_i\left(\boldsymbol{y}\right)\right)$. They can be expressed as

$$\boldsymbol{S}_i^c = \boldsymbol{S}_i\left(\boldsymbol{K}_i\left(\boldsymbol{y}^c\right)\right) \tag{44}$$

$$\begin{aligned}\Delta_1\boldsymbol{S}_i^I &= \sum_{r=1}^{n}\frac{\partial\boldsymbol{S}_i\left(\boldsymbol{K}_i\left(\boldsymbol{y}^c\right)\right)}{\partial\boldsymbol{K}_i\left(\boldsymbol{y}^c\right)}\cdot\frac{\partial\boldsymbol{K}_i\left(\boldsymbol{y}^c\right)}{\partial y_r}\left(y_r^I - y_r^c\right)\\ &= \sum_{r=1}^{n}\frac{\partial\boldsymbol{S}_i\left(\boldsymbol{K}_i\left(\boldsymbol{y}^c\right)\right)}{\partial\boldsymbol{K}_i\left(\boldsymbol{y}^c\right)}\cdot\frac{\partial\boldsymbol{K}_i\left(\boldsymbol{y}^c\right)}{\partial y_r}\Delta y_r\delta_r\end{aligned} \tag{45}$$

where y_r^c and Δy_r are the midpoint value and interval radius of the interval parameter y_r. $\boldsymbol{y}^c$ is the midpoint value of the interval parameter vector. $\boldsymbol{S}_i^c$ and $\Delta_1\boldsymbol{S}_i^I$ are the midpoint value and deviation interval of the composite function matrix $\boldsymbol{S}_i\left(\boldsymbol{K}_i\left(\boldsymbol{y}\right)\right)$, respectively.

The transition parameter δ_r denotes a fixed interval, i.e., the standard interval variable $\delta_r = [-1, +1]$.

Similarly, using first-order Taylor series expansion, the composite function vector $\boldsymbol{T}_i\left(\boldsymbol{K}_i\left(\boldsymbol{y}\right)\right)$ at the midpoints of the interval parameter vector $\boldsymbol{y}$ can be expressed as

$$\boldsymbol{T}_i\left(\boldsymbol{K}_i\left(\boldsymbol{y}\right)\right) = \boldsymbol{T}_i^c + \Delta_1\boldsymbol{T}_i^I \tag{46}$$

where $\boldsymbol{T}_i^c$ and $\Delta_1\boldsymbol{T}_i^I$ are the midpoint value and deviation interval of the composite function vector $\boldsymbol{T}_i\left(\boldsymbol{K}_i\left(\boldsymbol{y}\right)\right)$. They can be expressed as

$$\boldsymbol{T}_i^c = \boldsymbol{T}_i\left(\boldsymbol{K}_i\left(\boldsymbol{y}^c\right)\right) \tag{47}$$

$$\begin{aligned}\Delta_1\boldsymbol{T}_i^I &= \sum_{r=1}^{n}\frac{\partial\boldsymbol{T}_i\left(\boldsymbol{K}_i\left(\boldsymbol{y}^c\right)\right)}{\partial\boldsymbol{K}_i\left(\boldsymbol{y}^c\right)}\cdot\frac{\partial\boldsymbol{K}_i\left(\boldsymbol{y}^c\right)}{\partial y_r}\left(y_r^I - y_r^c\right)\\ &= \sum_{r=1}^{n}\frac{\partial\boldsymbol{T}_i\left(\boldsymbol{K}_i\left(\boldsymbol{y}^c\right)\right)}{\partial\boldsymbol{K}_i\left(\boldsymbol{y}^c\right)}\cdot\frac{\partial\boldsymbol{K}_i\left(\boldsymbol{y}^c\right)}{\partial y_r}\Delta y_r\delta_r\end{aligned} \tag{48}$$

It is noted that the accuracy of the first-order Taylor series expansion decreases when the levels of uncertainty of uncertain parameters increase gradually.

Using the perturbation theory, substituting Eqs. (43) and (46) into Eq. (42), one yields

$$\boldsymbol{\gamma}_i^I = \left(\boldsymbol{T}_i^c + \Delta_1\boldsymbol{T}_i^I\right)^{-1}\left(\boldsymbol{S}_i^c + \Delta_1\boldsymbol{S}_i^I\right) \tag{49}$$

According to the Neumann series expansion [26], if the spectral radius of $\left(\boldsymbol{T}_i^c\right)^{-1}\Delta_1\boldsymbol{T}_i$ is less than 1, namely $\|\left(\boldsymbol{T}_i^c\right)^{-1}\Delta_1\boldsymbol{T}_i\| < 1$, $\left(\boldsymbol{T}_i^c + \Delta_1\boldsymbol{T}_i^I\right)^{-1}$ can be approximated by retaining the first two terms

$$\begin{aligned}\left(\boldsymbol{T}_i^c + \Delta_1\boldsymbol{T}_i^I\right)^{-1} &= \left(\boldsymbol{T}_i^c\right)^{-1} - \left(\boldsymbol{T}_i^c\right)^{-1}\Delta_1\boldsymbol{T}_i^I\left(\boldsymbol{T}_i^c\right)^{-1}\\ &\quad + \left(\left(\boldsymbol{T}_i^c\right)^{-1}\Delta_1\boldsymbol{T}_i^I\right)^2\left(\boldsymbol{T}_i^c\right)^{-1}\end{aligned} \tag{50}$$

Substituting Eqs. (50) into (49), using the first-order perturbation term and neglecting the higher-order terms, one obtains

$$\begin{aligned}\boldsymbol{\gamma}_i^I \approx\ &\left(\boldsymbol{T}_i^c\right)^{-1}\boldsymbol{S}_i^c + \left(\boldsymbol{T}_i^c\right)^{-1}\Delta_1\boldsymbol{S}_i^I\\ &- \left(\boldsymbol{T}_i^c\right)^{-1}\Delta_1\boldsymbol{T}_i^I\left(\boldsymbol{T}_i^c\right)^{-1}\boldsymbol{S}_i^c\end{aligned} \tag{51}$$

Thus, Eq. (51) can be rewritten as

$$\boldsymbol{\gamma}_i^I = \boldsymbol{\gamma}_i^c + \Delta_1\boldsymbol{\gamma}_i^I \tag{52}$$

where $\boldsymbol{\gamma}_i^c$ and $\Delta_1\boldsymbol{\gamma}_i^I$ are the midpoint value and deviation interval of the interval luffing angular response vector $\boldsymbol{\gamma}_i^I$. They can be expressed as

$$\boldsymbol{\gamma}_i^c = \left(\boldsymbol{T}_i^c\right)^{-1} \boldsymbol{S}_i^c \tag{53}$$

$$\begin{aligned}\Delta_1\boldsymbol{\gamma}_i^I &= \left(\boldsymbol{T}_i^c\right)^{-1} \Delta_1\boldsymbol{S}_i^I - \left(\boldsymbol{T}_i^c\right)^{-1} \Delta_1\boldsymbol{T}_i^I \left(\boldsymbol{T}_i^c\right)^{-1} \boldsymbol{S}_i^c \\ &= \left(\boldsymbol{T}_i^c\right)^{-1} \left[\Delta_1\boldsymbol{S}_i^I - \Delta_1\boldsymbol{T}_i^I \left(\boldsymbol{T}_i^c\right)^{-1} \boldsymbol{S}_i^c\right] \\ &= \left(\boldsymbol{T}_i^c\right)^{-1} \left[\sum_{r=1}^{n} \left(\frac{\partial \boldsymbol{S}_i\left(\boldsymbol{K}_i\left(\boldsymbol{y}^c\right)\right)}{\partial \boldsymbol{K}_i\left(\boldsymbol{y}^c\right)} \cdot \frac{\partial \boldsymbol{K}_i\left(\boldsymbol{y}^c\right)}{\partial y_r} \right.\right. \\ &\quad \left.\left. - \frac{\partial \boldsymbol{T}_i\left(\boldsymbol{K}_i\left(\boldsymbol{y}^c\right)\right)}{\partial \boldsymbol{K}_i\left(\boldsymbol{y}^c\right)} \cdot \frac{\partial \boldsymbol{K}_i\left(\boldsymbol{y}^c\right)}{\partial y_r} \left(\boldsymbol{T}_i^c\right)^{-1} \boldsymbol{S}_i^c\right) \Delta y_r \delta_r\right] \\ &= \Delta_1\boldsymbol{\gamma}_i \cdot \delta_r \end{aligned} \tag{54}$$

Therefore, according to interval union operation and based on the monotonicity of $\Delta_1\boldsymbol{\gamma}_i^I$ with respect to δ_r, the interval radius $\Delta_1\boldsymbol{\gamma}_i$ can be obtained as

$$\begin{aligned}\Delta_1\boldsymbol{\gamma}_i = \sum_{r=1}^{n} \left| \left(\boldsymbol{T}_i^c\right)^{-1} \left(\frac{\partial \boldsymbol{S}_i\left(\boldsymbol{K}_i\left(\boldsymbol{y}^c\right)\right)}{\partial \boldsymbol{K}_i\left(\boldsymbol{y}^c\right)} \cdot \frac{\partial \boldsymbol{K}_i\left(\boldsymbol{y}^c\right)}{\partial y_r} \right.\right. \\ \left.\left. - \frac{\partial \boldsymbol{T}_i\left(\boldsymbol{K}_i\left(\boldsymbol{y}^c\right)\right)}{\partial \boldsymbol{K}_i\left(\boldsymbol{y}^c\right)} \cdot \frac{\partial \boldsymbol{K}_i\left(\boldsymbol{y}^c\right)}{\partial y_r} \left(\boldsymbol{T}_i^c\right)^{-1} \boldsymbol{S}_i^c\right) \Delta y_r \right|\end{aligned} \tag{55}$$

where $|\blacksquare|$ denotes the absolute value.

Due to the interval radius Δy_r derived from interval luffing angular response vector $\boldsymbol{\gamma}_i^I$ is included in the above formula, the luffing angular response field is not deterministic value but an interval.

Therefore, the upper bound $\overline{\boldsymbol{\gamma}_i}$ and lower bound $\underline{\boldsymbol{\gamma}_i}$ of the interval luffing angular response vector $\boldsymbol{\gamma}_i^I$ with respect to the interval parameter vector $\boldsymbol{y}$ can be expressed as

$$\overline{\boldsymbol{\gamma}_i} = \boldsymbol{\gamma}_i^c + \Delta_1\boldsymbol{\gamma}_i \tag{56}$$

$$\underline{\boldsymbol{\gamma}_i} = \boldsymbol{\gamma}_i^c - \Delta_1\boldsymbol{\gamma}_i \tag{57}$$

Combining with dynamics-based nonsingular interval model, Fig. 4 shows the detailed steps and the procedure of FCFIPM for the DACS can be summarized as follows

Step 1: Generate initial sample y_r, based on the deterministic dynamic model (see Eq. 30), identifying reasonable lower bound $\underline{y_r}$ and upper bound $\overline{y_r}$ for every interval variable y_r^I (see Eq. 36):

1. Find the maximum upper bound $\overline{y_r}$ of y_r^I using $\nexists \frac{\partial f\left(y_1^c,\ldots,\overline{y_r}+\sigma,\ldots,y_n^c,t\right)}{\partial t}$ and $\exists \frac{\partial f\left(y_1^c,\ldots,\overline{y_r},\ldots,y_n^c,t\right)}{\partial t}$.
2. Find the minimum lower bound $\underline{y_r}$ of y_r^I using $\nexists \frac{\partial f\left(y_1^c,\ldots,\underline{y_r}-\sigma,\ldots,y_n^c,t\right)}{\partial t}$ and $\exists \frac{\partial f\left(y_1^c,\ldots,\underline{y_r},\ldots,y_n^c,t\right)}{\partial t}$.
3. If r $< n$, let r = r + 1; otherwise, r = n, go to next step.

Step 2: Construct dynamics-based nonsingular interval model $\boldsymbol{Y}^{\boldsymbol{I}} = \left(y_1^{\mathrm{I}},\ldots,y_r^{\mathrm{I}},\ldots,y_n^{\mathrm{I}}\right)$.

Step 3: To produce the luffing angular response equilibrium equation (see Eq. 37) of the DACS with nonsingularity.

Step 4: Based on differential property of composite function and perturbation theory, performing the decompositions of composite function matrix $\boldsymbol{S}_i\left(\boldsymbol{K}_i\left(\boldsymbol{y}\right)\right)$ (see Eqs. 43–45) and composite function vector $\boldsymbol{T}_i\left(\boldsymbol{K}_i\left(\boldsymbol{y}\right)\right)$ (see Eqs. 46–48) by first-order Taylor series expansion.

Step 5: Evaluating the inverse of composite function vector $\boldsymbol{T}_i\left(\boldsymbol{K}_i\left(\boldsymbol{y}\right)\right)$ in approximate terms by Neumann series expansion (see Eq. 50).

Step 6: Calculating interval luffing angular response vector $\boldsymbol{\gamma}_i^I$ (see Eq. 52), the midpoint value $\boldsymbol{\gamma}_i^c$ (see Eq. 53) and deviation interval $\Delta_1\boldsymbol{\gamma}_i^I$ (see Eq. 54) of the interval luffing angular response vector $\boldsymbol{\gamma}_i^I$.

Step 7: Calculating the upper bound $\overline{\boldsymbol{\gamma}_i}$ (see Eq. 56) and lower bound $\underline{\boldsymbol{\gamma}_i}$ (see Eq. 57) of the interval luffing angular response vector $\boldsymbol{\gamma}_i^I$.

It is worth emphasizing that the proposed FCFIPM requires to explore dynamics-based nonsingular interval model at first, in order to obtain reasonable maximum interval for every uncertain structure parameters, which can enhance the reliability of the system greatly and provide reference for setting reasonable interval change ratios of interval variables.

6 Numerical examples

In this section, some examples were carried out with MATLAB for the DACS to illustrate the feasibility and effectiveness of the proposed method in this paper. The first one is presented to analyze the influence of the system parameters on the dynamics of the DACS with deterministic parameters. The second one is to construct the dynamics-based nonsingular interval model under the same spatial trajectory. Based on the above analysis, the third one is presented to demonstrate the feasibility of the MHUM for solving the luffing angular response field problem of the DACS with narrowly bounded structure parameters. The Monte Carlo method is applied as a referenced approach for validating the feasible and efficiency of the proposed MHRM.

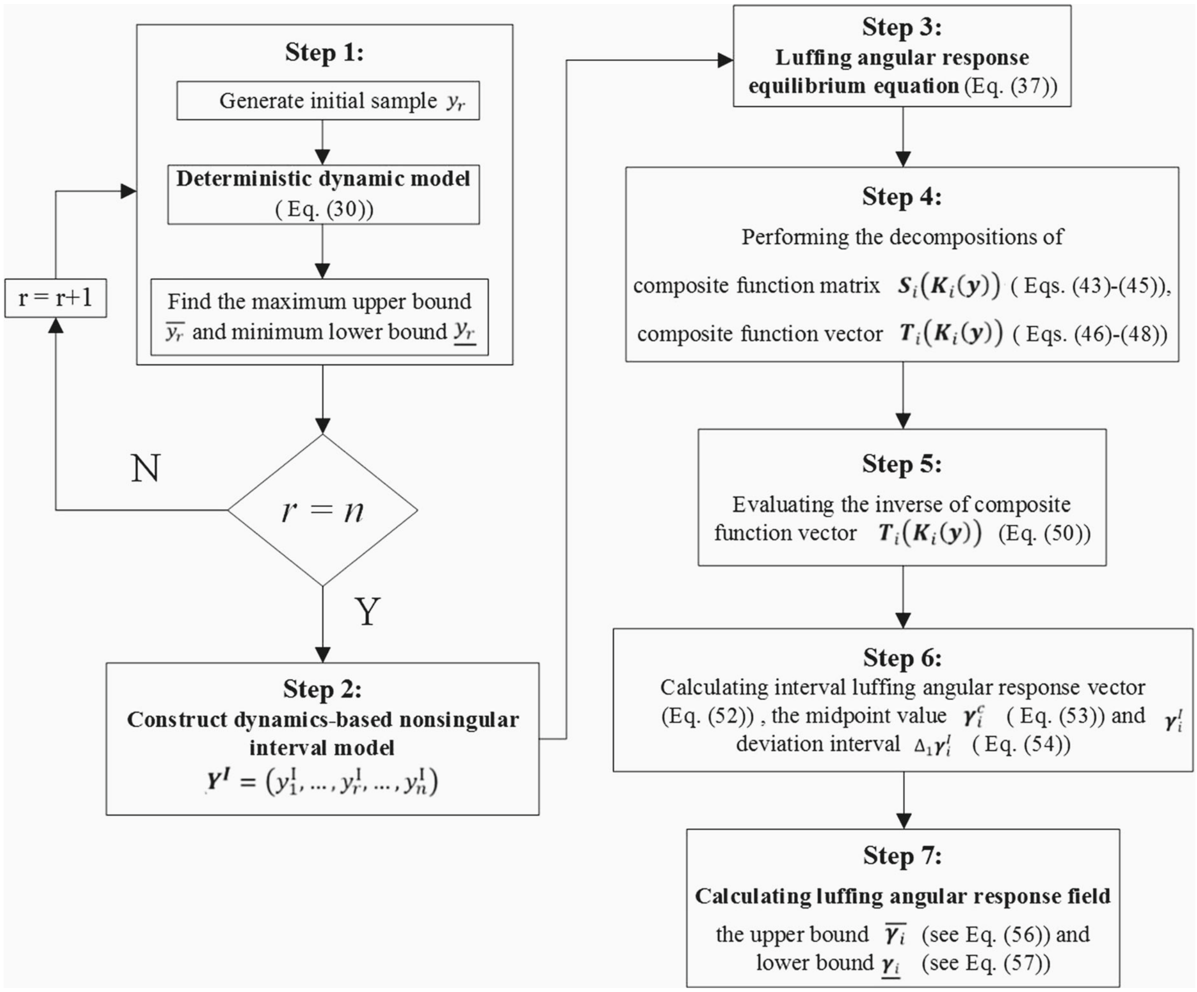

Fig. 4 Flowchart of the proposed FCFIPM

6.1 Deterministic kinematic and dynamic responses analysis

In this section, in order to investigate the effect of the deterministic system parameters on the kinematic and dynamic responses of the DACS, the deterministic system parameters of DACS are listed in Table 1.

During the simulation, by referring to the engineering practice, let the centroid of the payload move from the initial coordinate (0, 0.5 m, 0°) to terminal coordinate (−0.5, 0 m, 30°) along the spatial trajectory formulated as

$$\begin{cases} y = -0.5 * \sin(pi/2 * t) \\ z = 0.5 * \cos(pi/2 * t) \\ \theta = pi/6 * t \end{cases} \tag{58}$$

Table 1 Deterministic DACS parameters

Symbol	Description	Value
D (m)	Length of A_1A_2	12
d (m)	Length of payload	2.5
L_1 (m)	Length of lifting arm A_1B_1	5
L_2 (m)	Length of lifting arm A_2B_2	5
S_1 (m)	Length of hoisting rope B_1C_1 at the terminal location	1
S_2 (m)	Length of hoisting rope B_2C_2 at the terminal location	1
m_1 (kg)	Mass of lifting arm A_1B_1	50,000
m_2 (kg)	Mass of lifting arm A_2B_2	50,000
m_p (kg)	Mass of payload C_1C_2	50,000

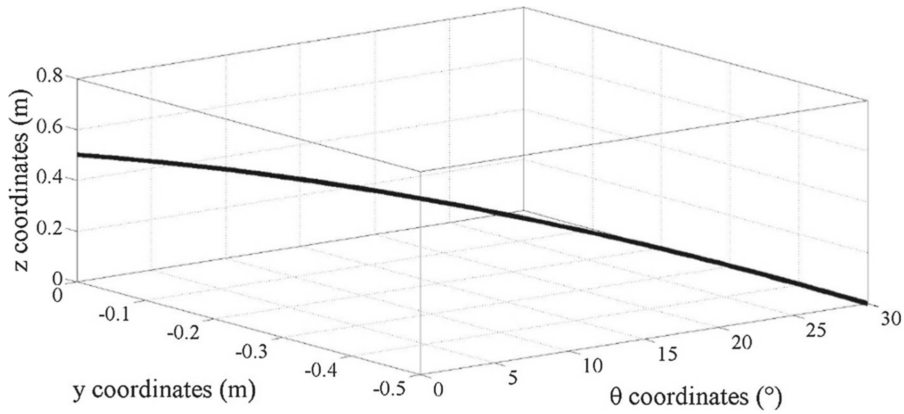

Fig. 5 Trajectory of the payload

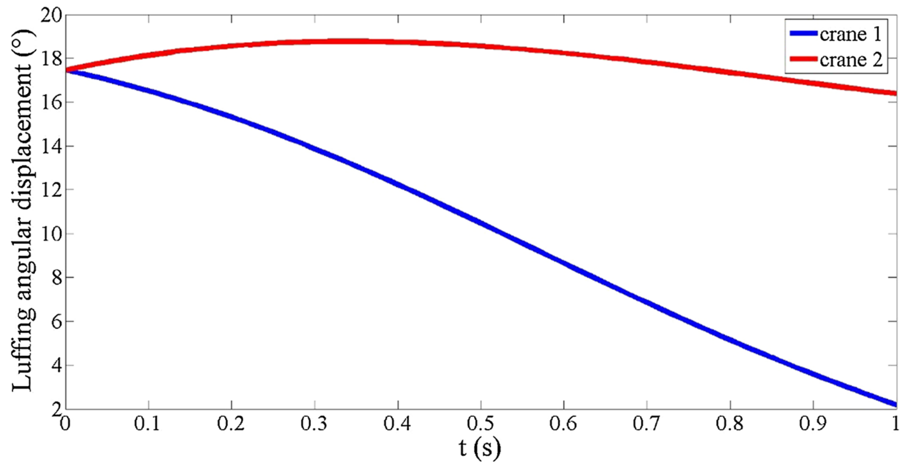

Fig. 6 Luffing angular displacement of the DACS

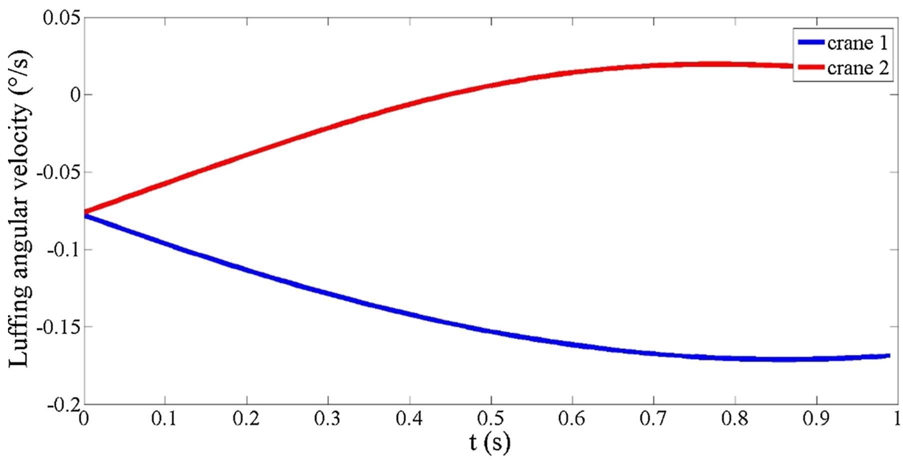

Fig. 7 Luffing angular velocity of the DACS

The spatial trajectory of the payload in Eq. (58) is a smooth curve shown in Fig. 5. It is noted that the trajectory in Eq. 58 is a reference trajectory.

Figures 6, 7 and 8 show the curves of the luffing angular displacement γ_i $(i = 1, 2)$, luffing angular velocity $\dot{\gamma}_i$ and luffing angular acceleration $\ddot{\gamma}_i$ of the DACS, respectively. It can be seen that all the curves of the two lifting arms change smoothly and reasonable numerical results are obtained. In other words, one can observe that the DACS possesses a

Fig. 8 Luffing angular acceleration of the DACS

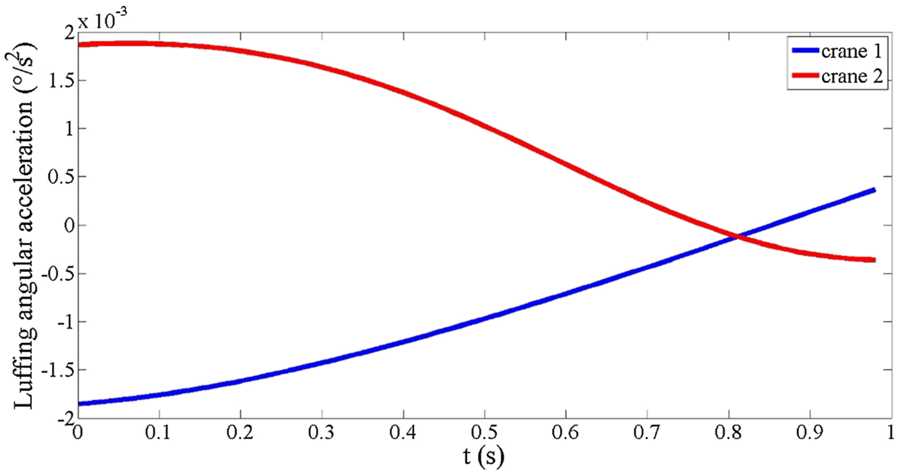

Fig. 9 Driving torques of the DACS

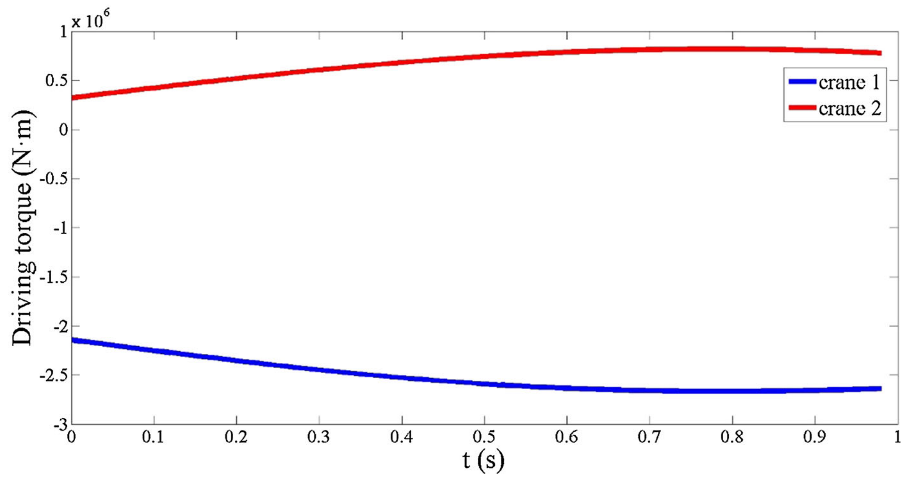

good kinematic behavior in terms of angular displacement, angular velocity and angular acceleration of the luffing angle. Furthermore, appropriate state of lifting arms is also theoretical references for controlling the operation of the payload stably and reliably, as well as effectively reducing the acute vibration of hoisting ropes.

The driving torques of the DACS and the sum of the absolute value of driving torques are plotted in Figs. 9 and 10, respectively. It can be seen that the driving torque of crane 1 is much larger than that of crane 2; besides, the driving torque of crane 1 and crane 2 present increases at first and decreases subsequently. Furthermore, the maximum sum of the absolute value of driving torques of the DACS appears when the time is equal to nearly 0.8 s.

6.2 Dynamics-based nonsingular interval model

In this section, in order to investigate allowable ranges of uncertain structure parameters (D, d, L_1, L_2) and the impact of those on the dynamic response, the actual analysis process of the dynamics-based nonsingular interval model can be divided into two steps. The first step is to obtain the dynamic response with given deterministic parameters. Subsequently, considering the significance of structure parameters on dynamic response, we settle out the allowable ranges of structure parameters in the second step. Meantime, we give results of the effect of the structure parameters on the dynamic responses of the DACS with deterministic parameters. Thus, a dynamics-based nonsingular interval model (Eq. (32) as illustrated in Sect. 4.1) can be constructed.

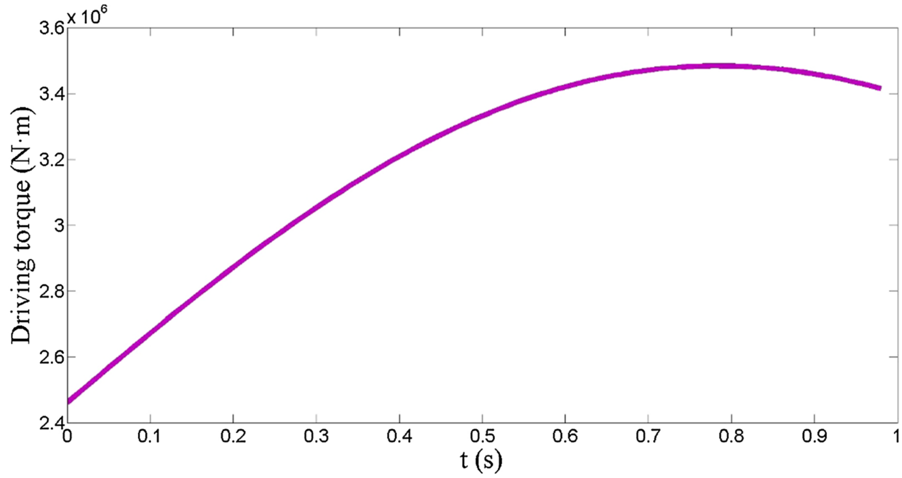

Fig. 10 Sum of the absolute value of driving torques

The results are shown in Figs. 11, 12, 13, 15 and 16, respectively. During the simulation, let the centroid of the payload move along the same spatial trajectory as stated in Sect. 6.1.

Figures 11 and 12 depict the effect of different D (the length of A_1A_2) on driving torque of the crane 1 and crane 2, respectively. As shown in the six curves of every figure consistently, we can see that two red curves ($D = 11\,\mathrm{m}$ and $D = 13.5\,m$) are obviously different from other four blue curves ($D = 12,\ 12.5,\ 13,\ 13.5\,\mathrm{m}$). The notable characteristic is that each of two red curves has a singularity point. For the curves of $D = 11\,\mathrm{m}$ and $D = 13.5\,\mathrm{m}$, the singularity points appear when the time is equal to 0.48 and 0.63 s, respectively. However, other four blue curves are sufficiently smooth and have no singularity point, which indicate that the allowable range of the length of A_1A_2 is from 11.5 to 13 m.

Figures 13 and 14 depict the effect of different d (the length of C_1C_2) on driving torque of the crane 1 and crane 2, respectively. As shown in the six curves of every figure consistently, we can see that two red curves ($d = 1\,\mathrm{m}$ and $d = 4\,\mathrm{m}$) are obviously different from other five blue curves ($d = 1.5,\ 2,\ 2.5,\ 3,\ 3.5\,\mathrm{m}$). The notable characteristic is that each of two red curves has a singularity point. For the curves of $d = 1\,\mathrm{m}$ and $d = 4\,\mathrm{m}$, the singularity points appear when the time is equal to 0.86s and 0.03s, respectively. However, other five blue curves are sufficiently smooth and have no singularity point, which indicate that the allowable range of the length of payload C_1C_2 is from 1.5 to 3.5 m.

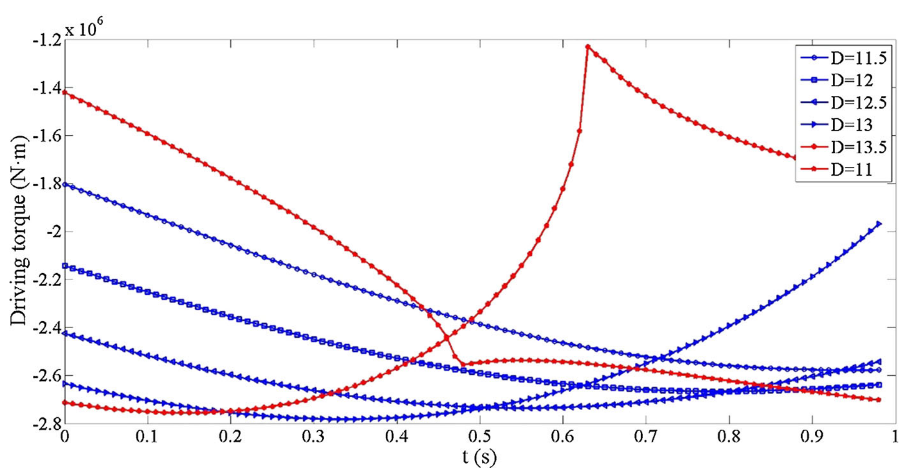

Fig. 11 Effect of the length of A_1A_2 on driving torque of the crane 1

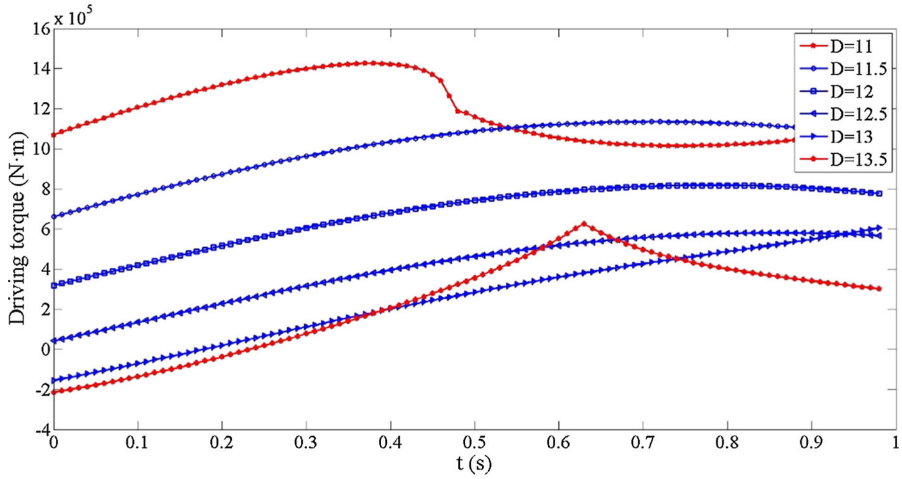

Fig. 12 Effect of the length of A_1A_2 on driving torque of the crane 2

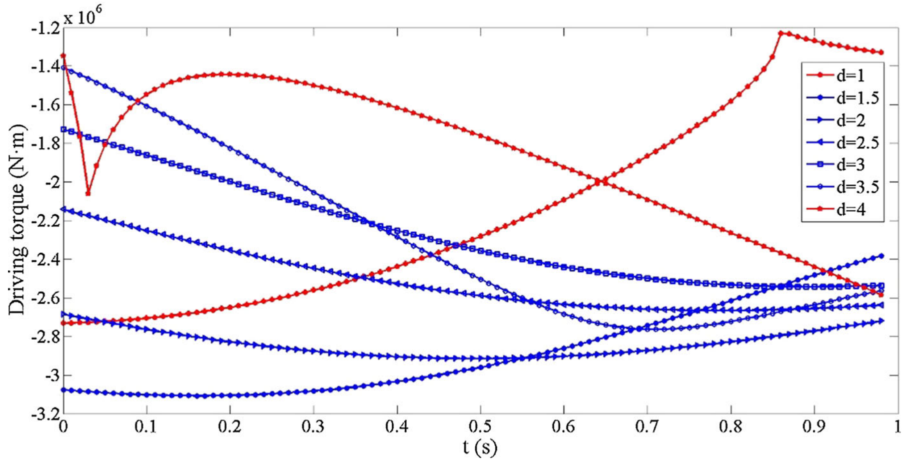

Fig. 13 Effect of the length of payload C_1C_2 on driving torque of the crane 1

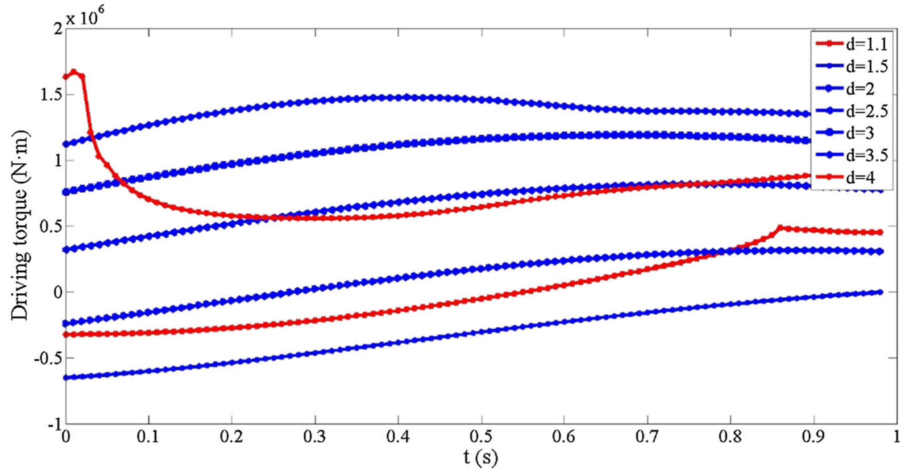

Fig. 14 Effect of the length of payload C_1C_2 on driving torque of the crane 2

Figure 15 depicts the effect of different L_1 (the length of lifting arm A_1B_1) on driving torque of the crane 1. As shown in the five curves, we can see that two red curves ($L_1 = 4\,\text{m}$ and $L_1 = 6\,\text{m}$) are obviously different from other three blue curves ($L_1 = 4.5,\ 5,\ 5.5\,\text{m}$). The notable characteristic is that

Fig. 15 Effect of the length of lifting arm A_1B_1 on driving torque of the crane 1

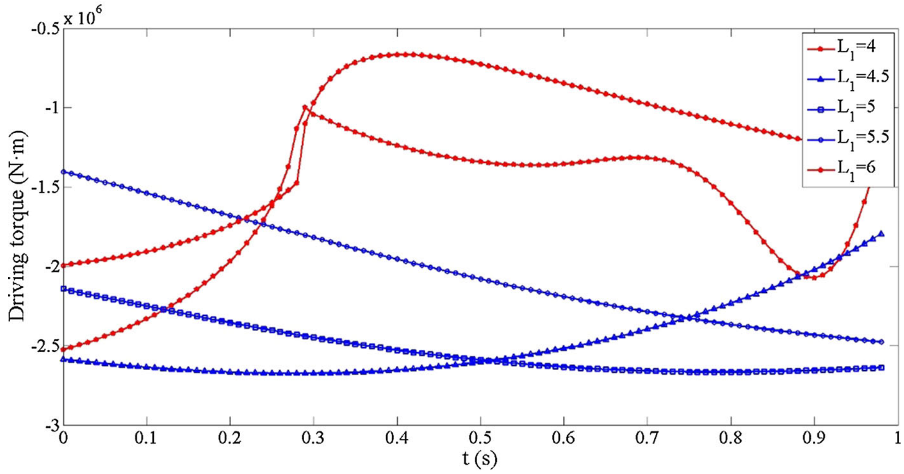

Fig. 16 Effect of the length of lifting arm A_2B_2 on driving torque of the crane 2

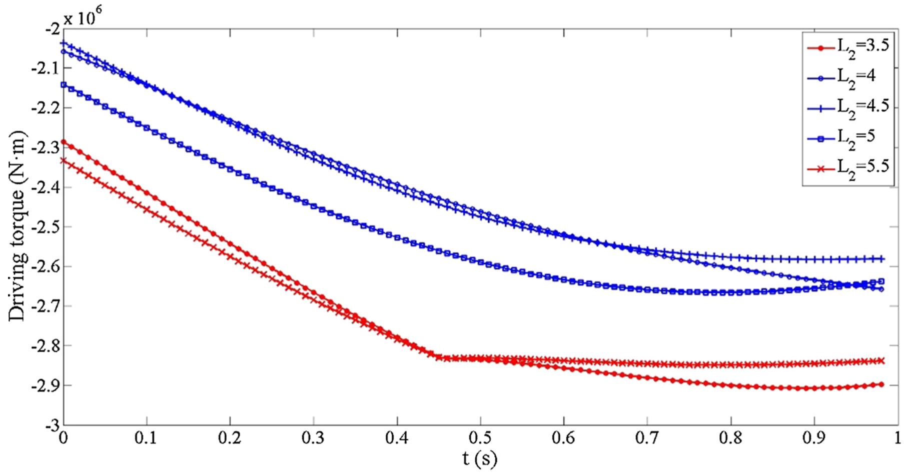

each of two red curves has a singularity point. For the curves of $L_1 = 4\,\mathrm{m}$ and $L_1 = 6\,\mathrm{m}$, the singularity points appear when the time is equal to 0.29 and 0.27 s, respectively. However, other three blue curves are sufficiently smooth and have no singularity point, which indicate that the allowable range of the length of lifting arm A_1B_1 is from 4.5 to 5.5 m.

Figure 16 depicts the effect of different L_2 (the length of lifting arm A_2B_2) on driving torque of the crane 2. As shown in the five curves, we can see that two red curves ($L_2 = 3.5\,\mathrm{m}$ and $L_2 = 5.5\,\mathrm{m}$) are obviously different from other three blue curves ($L_2 = 4,\ 4.5,\ 5\,\mathrm{m}$). The notable characteristic is that each of two red curves has a singularity point. For the curves of $L_2 = 3.5\,\mathrm{m}$ and $L_2 = 5.5\,\mathrm{m}$, the singularity points appear when the time is equal to 0.44 and 0.46 s, respectively. However, other three blue curves are sufficiently smooth and have no singularity point, which indicate that the allowable range of the length of lifting arm A_2B_2 is from 4 to 5 m.

In order to describe the obtained dynamics-based nonsingular interval model constituting of reasonable interval parameters clearly, the maximum dispersal degree (MDD) of an interval variable can be defined in the following formula

$$x^I_{MDD} = \frac{x^c}{\Delta x} = \frac{x^U - x^L}{x^U - x^L} \tag{59}$$

where x^c and Δx are the midpoint value (MV) and interval radius of the interval variable x^I. x^L and x^U are the lower bound (LB) and upper bound (UB) of the interval variable x^I.

Based on above analysis, a dynamics-based nonsingular interval model can be constructed as listed in Table 2.

Table 2 Dynamics-based nonsingular interval model

Interval variables	LB	UB	MV	MDD
D^I (m)	11.5	13	12.75	0.06
d^I (m)	1.5	3.5	2.5	0.40
L_1^I (m)	4.5	5.5	5	0.10
L_2^I (m)	4	5	4.5	0.11

6.3 Luffing angular response field problem of DACS with interval parameters

In this section, in order to investigate the feasibility and effectiveness of the proposed method described in Sect. 5 on the interval DACS response field problem, based on the analysis in Sect. 6.2, the uncertain structure parameters (D, d, L_1, L_2) are considered as narrowly interval parameters. These interval parameters are supposed to be independent with each other. Meantime, we consider other system parameters as specific deterministic parameters. The properties of these deterministic and interval parameters are listed in Table 3.

Based on above description, we have

$$\begin{aligned}
&\boldsymbol{y} = \{y_1, y_2, y_3, y_4\}^{\mathrm{T}} = \{D, d, L_1, L_2\}^{\mathrm{T}},\\
&\boldsymbol{y}^{\boldsymbol{c}} = \left\{y_1^c, y_2^c, y_3^c, y_4^c\right\}^{\mathrm{T}} = \left\{D^c, d^c, L_1^c, L_2^c\right\}^{\mathrm{T}},\\
&\Delta y_r = \{\Delta y_1, \Delta y_2, \Delta y_3, \Delta y_4\}^{\mathrm{T}}\\
&\quad = \{\Delta D, \Delta d, \Delta L_1, \Delta L_2\}^{\mathrm{T}}. \qquad (60)
\end{aligned}$$

where ΔD, Δd, ΔL_1 and ΔL_2 are the interval radius of interval variables D, d, L_1 and L_2, respectively.

Substituting Eqs. (60) into (8), one obtains

$$\begin{aligned}
K_{11}^c &= -2L_1^c\left(z - \frac{d^c \sin\theta}{2}\right),\\
K_{21}^c &= -2L_1^c\left(y - \frac{d^c \cos\theta}{2} + \frac{D^c}{2}\right),\\
K_{31}^c &= \left(y - \frac{d^c \cos\theta}{2} + \frac{D^c}{2}\right)^2\\
&\quad + \left(z - \frac{d^c \sin\theta}{2}\right)^2 + \left(L_1^c\right)^2 - S_1^2,\\
K_{12}^c &= -2L_2^c\left(z + \frac{d^c \sin\theta}{2}\right),\\
K_{22}^c &= -2L_2^c\left(y + \frac{d^c \cos\theta}{2} - \frac{D^c}{2}\right),\\
K_{32}^c &= \left(y + \frac{d^c \cos\theta}{2} - \frac{D^c}{2}\right)^2\\
&\quad + \left(z + \frac{d^c \sin\theta}{2}\right)^2 + \left(L_2^c\right)^2 - S_2^2. \qquad (61)
\end{aligned}$$

where $\blacksquare^c$ is the symbol of midpoint value.

Substituting Eqs. (61) into (35), one obtains

$$\begin{aligned}
\boldsymbol{S}_1^c &= \sqrt{\left(K_{11}^c\right)^2 + \left(K_{21}^c\right)^2 - \left(K_{31}^c\right)^2} - \left(K_{11}^c\right),\\
\boldsymbol{T}_1^c &= K_{31}^c - K_{21}^c;\\
\boldsymbol{S}_2^c &= \sqrt{\left(K_{12}^c\right)^2 + \left(K_{22}^c\right)^2 - \left(K_{32}^c\right)^2} - \left(K_{12}^c\right),\\
\boldsymbol{T}_2^c &= K_{32}^c - K_{22}^c. \qquad (62)
\end{aligned}$$

Table 3 DACS parameters

System parameters	Symbol	Description	Constant or midpoint values
Deterministic parameters	m_1 (kg)	Mass of lifting arm A_1B_1	50,000
	m_2 (kg)	Mass of lifting arm A_2B_2	50,000
	m_p (kg)	Mass of payload C_1C_2	50,000
	S_1 (m)	Length of hoisting rope B_1C_1	1
	S_2 (m)	Length of hoisting rope B_2C_2	1
	y (m)	Y-axis coordinate of centroid O_p	$y = 0.5$
	z (m)	Z-axis coordinate of centroid O_p	$z = 0.5$
	θ (°)	Orientation coordinate of centroid O_p	$\theta = pi/6$
Interval parameters	D^c (m)	Midpoint of length of A_1A_2	12.75
	d^c (m)	Midpoint of length of payload C_1C_2	2.5
	L_1^c (m)	Midpoint of length of lifting arm A_1B_1	5
	L_2^c (m)	Midpoint of length of lifting arm A_2B_2	4.5

Substituting Eqs. (62) into (53), the midpoint value $\boldsymbol{\gamma}_i^c$ of the interval luffing angular response vector can be obtained as

$$\boldsymbol{\gamma}_1^c = \left(\boldsymbol{T}_1^c\right)^{-1}\boldsymbol{S}_1^c,$$
$$\boldsymbol{\gamma}_2^c = \left(\boldsymbol{T}_2^c\right)^{-1}\boldsymbol{S}_2^c. \tag{63}$$

For the crane 1, $\frac{\partial \boldsymbol{S}_1(\boldsymbol{K}_1(\boldsymbol{y}^c))}{\partial \boldsymbol{K}_1(\boldsymbol{y}^c)}$ is composed of $\frac{\partial \boldsymbol{S}_1(\boldsymbol{K}_1(\boldsymbol{y}^c))}{\partial K_{11}(\boldsymbol{y}^c)}$, $\frac{\partial \boldsymbol{S}_1(\boldsymbol{K}_1(\boldsymbol{y}^c))}{\partial K_{21}(\boldsymbol{y}^c)}$ and $\frac{\partial \boldsymbol{S}_1(\boldsymbol{K}_1(\boldsymbol{y}^c))}{\partial K_{31}(\boldsymbol{y}^c)}$, based on the partial derivation law, one obtains

$$\frac{\partial \boldsymbol{S}_1\left(\boldsymbol{K}_1\left(\boldsymbol{y}^c\right)\right)}{\partial K_{11}\left(\boldsymbol{y}^c\right)} = \frac{K_{11}^c}{\sqrt{\left(K_{11}^c\right)^2+\left(K_{21}^c\right)^2-\left(K_{31}^c\right)^2}}-1,$$
$$\frac{\partial \boldsymbol{S}_1\left(\boldsymbol{K}_1\left(\boldsymbol{y}^c\right)\right)}{\partial K_{21}\left(\boldsymbol{y}^c\right)} = \frac{K_{21}^c}{\sqrt{\left(K_{11}^c\right)^2+\left(K_{21}^c\right)^2-\left(K_{31}^c\right)^2}},$$
$$\frac{\partial \boldsymbol{S}_1\left(\boldsymbol{K}_1\left(\boldsymbol{y}^c\right)\right)}{\partial K_{31}\left(\boldsymbol{y}^c\right)} = \frac{-K_{31}^c}{\sqrt{\left(K_{11}^c\right)^2+\left(K_{21}^c\right)^2-\left(K_{31}^c\right)^2}}. \tag{64}$$

Similarly, $\frac{\partial \boldsymbol{T}_1(\boldsymbol{K}_1(\boldsymbol{y}^c))}{\partial \boldsymbol{K}_1(\boldsymbol{y}^c)}$ is composed of $\frac{\partial \boldsymbol{T}_1(\boldsymbol{K}_1(\boldsymbol{y}^c))}{\partial K_{11}(\boldsymbol{y}^c)}$, $\frac{\partial \boldsymbol{T}_1(\boldsymbol{K}_1(\boldsymbol{y}^c))}{\partial K_{21}(\boldsymbol{y}^c)}$ and $\frac{\partial \boldsymbol{T}_1(\boldsymbol{K}_1(\boldsymbol{y}^c))}{\partial K_{31}(\boldsymbol{y}^c)}$, one obtains

$$\frac{\partial \boldsymbol{T}_1\left(\boldsymbol{K}_1\left(\boldsymbol{y}^c\right)\right)}{\partial K_{11}\left(\boldsymbol{y}^c\right)} = 0,\ \frac{\partial \boldsymbol{T}_1\left(\boldsymbol{K}_1\left(\boldsymbol{y}^c\right)\right)}{\partial K_{21}\left(\boldsymbol{y}^c\right)} = -1,$$
$$\frac{\partial \boldsymbol{T}_1\left(\boldsymbol{K}_1\left(\boldsymbol{y}^c\right)\right)}{\partial K_{31}\left(\boldsymbol{y}^c\right)} = 1. \tag{65}$$

Here, let us introduce the interval change ratios D_F, d_F, L_{1F} and L_{2F} for interval variables D, d, L_1 and L_2, respectively, they can be expressed as follows

$$\Delta D = D^c \cdot D_F,\ \Delta d = d^c \cdot d_F,\ \Delta L_1 = L_1^c \cdot L_{1F},$$
$$\Delta L_2 = L_2^c \cdot L_{2F}. \tag{66}$$

Substituting Eqs. (61)–(65) into (55), the interval radius $\Delta_1\boldsymbol{\gamma}_1$ of the interval luffing angular response vector can be obtained as

$$\Delta_1\boldsymbol{\gamma}_1 = \left|\left(\boldsymbol{T}_1^c\right)^{-1}\left(\sum_{r=1}^{4}\frac{\partial \boldsymbol{S}_1\left(\boldsymbol{K}_1\left(\boldsymbol{y}^c\right)\right)}{\partial \boldsymbol{K}_1\left(\boldsymbol{y}^c\right)}\cdot\frac{\partial \boldsymbol{K}_1\left(\boldsymbol{y}^c\right)}{\partial y_r}\Delta y_r\right)\right.$$
$$\left.-\left(\boldsymbol{T}_1^c\right)^{-2}\boldsymbol{S}_1^c\left(\sum_{r=1}^{4}\frac{\partial \boldsymbol{T}_1\left(\boldsymbol{K}_1\left(\boldsymbol{y}^c\right)\right)}{\partial \boldsymbol{K}_1\left(\boldsymbol{y}^c\right)}\cdot\frac{\partial \boldsymbol{K}_1\left(\boldsymbol{y}^c\right)}{\partial y_r}\Delta y_r\right)\right| \tag{67}$$

where

$$\sum_{r=1}^{4}\frac{\partial \boldsymbol{S}_1\left(\boldsymbol{K}_1\left(\boldsymbol{y}^c\right)\right)}{\partial \boldsymbol{K}_1\left(\boldsymbol{y}^c\right)}\cdot\frac{\partial \boldsymbol{K}_1\left(\boldsymbol{y}^c\right)}{\partial y_r}\Delta y_r$$
$$= \left[\left(\frac{K_{21}^c}{\sqrt{\left(K_{11}^c\right)^2+\left(K_{21}^c\right)^2-\left(K_{31}^c\right)^2}}\right)\cdot\left(-L_1^c\right)\right.$$
$$+\left(\frac{-K_{31}^c}{\sqrt{\left(K_{11}^c\right)^2+\left(K_{21}^c\right)^2-\left(K_{31}^c\right)^2}}\right)$$
$$\left.\cdot\left(y-\frac{d^c\cos\theta}{2}+\frac{D^c}{2}\right)\right]\cdot\Delta D$$
$$+\left[\left(\frac{K_{11}^c}{\sqrt{\left(K_{11}^c\right)^2+\left(K_{21}^c\right)^2-\left(K_{31}^c\right)^2}}-1\right)\right.$$
$$\cdot\left(L_1^c\sin\theta\right)$$
$$+\left(\frac{K_{21}^c}{\sqrt{\left(K_{11}^c\right)^2+\left(K_{21}^c\right)^2-\left(K_{31}^c\right)^2}}\right)\cdot\left(L_1^c\cos\theta\right)$$
$$+\left(\frac{-K_{31}^c}{\sqrt{\left(K_{11}^c\right)^2+\left(K_{21}^c\right)^2-\left(K_{31}^c\right)^2}}\right)$$
$$\cdot\left(\left(y-\frac{d^c\cos\theta}{2}+\frac{D^c}{2}\right)(-\cos\theta)\right.$$
$$\left.\left.+\left(z-\frac{d^c\sin\theta}{2}\right)(-\sin\theta)\right)\right]\cdot\Delta d$$
$$+\left[\left(\frac{K_{11}^c}{\sqrt{\left(K_{11}^c\right)^2+\left(K_{21}^c\right)^2-\left(K_{31}^c\right)^2}}-1\right)\right.$$
$$\cdot\left(-2\left(z-\frac{d^c\sin\theta}{2}\right)\right)$$
$$+\left(\frac{K_{21}^c}{\sqrt{\left(K_{11}^c\right)^2+\left(K_{21}^c\right)^2-\left(K_{31}^c\right)^2}}\right)$$
$$\cdot\left(-2\left(y-\frac{d^c\cos\theta}{2}+\frac{D^c}{2}\right)\right)$$
$$\left.+\left(\frac{-K_{31}^c}{\sqrt{\left(K_{11}^c\right)^2+\left(K_{21}^c\right)^2-\left(K_{31}^c\right)^2}}\right)\cdot 2L_1^c\right]\cdot\Delta L_1 \tag{68}$$

$$\sum_{r=1}^{4}\frac{\partial \boldsymbol{T}_1\left(\boldsymbol{K}_1\left(\boldsymbol{y}^c\right)\right)}{\partial \boldsymbol{K}_1\left(\boldsymbol{y}^c\right)}\cdot\frac{\partial \boldsymbol{K}_1\left(\boldsymbol{y}^c\right)}{\partial y_r}\Delta y_r$$
$$= \left(L_1^c+y-\frac{d^c\cos\theta}{2}+\frac{D^c}{2}\right)\cdot\Delta D$$
$$+\left[-L_1^c\cos\theta+\left(y-\frac{d^c\cos\theta}{2}+\frac{D^c}{2}\right)\right.$$
$$(-\cos\theta)$$
$$\left.+\left(z-\frac{d^c\sin\theta}{2}\right)(-\sin\theta)\right]\cdot\Delta d$$

$$+\left[2\left(y-\frac{d^c\cos\theta}{2}+\frac{D^c}{2}\right)+2L_1^c\right]\cdot\Delta L_1 \tag{69}$$

In order to clarify the expressions, Eq. (68) can be rewritten as

$$\sum_{r=1}^{4}\frac{\partial \boldsymbol{S}_1\left(\boldsymbol{K}_1\left(\boldsymbol{y^c}\right)\right)}{\partial \boldsymbol{K}_1\left(\boldsymbol{y^c}\right)}\cdot\frac{\partial \boldsymbol{K}_1\left(\boldsymbol{y^c}\right)}{\partial x_r}\Delta y_r = \boldsymbol{S}_{1D}\cdot\Delta D+\boldsymbol{S}_{1d}\cdot\Delta d+\boldsymbol{S}_{1L_1}\cdot\Delta L_1 \tag{70}$$

where

$$\begin{aligned}
\boldsymbol{S}_{1D} =& \left(\frac{K_{21}^c}{\sqrt{\left(K_{11}^c\right)^2+\left(K_{21}^c\right)^2-\left(K_{31}^c\right)^2}}\right)\cdot\left(-L_1^c\right)\\
&+\left(\frac{-K_{31}^c}{\sqrt{\left(K_{11}^c\right)^2+\left(K_{21}^c\right)^2-\left(K_{31}^c\right)^2}}\right)\cdot\\
&\left(y-\frac{d^c\cos\theta}{2}+\frac{D^c}{2}\right),\\
\boldsymbol{S}_{1d} =& \left(\frac{K_{11}^c}{\sqrt{\left(K_{11}^c\right)^2+\left(K_{21}^c\right)^2-\left(K_{31}^c\right)^2}}-1\right)\\
&\cdot\left(L_1^c\sin\theta\right)\\
&+\left(\frac{K_{21}^c}{\sqrt{\left(K_{11}^c\right)^2+\left(K_{21}^c\right)^2-\left(K_{31}^c\right)^2}}\right)\\
&\cdot\left(L_1^c\cos\theta\right)\\
&+\left(\frac{-K_{31}^c}{\sqrt{\left(K_{11}^c\right)^2+\left(K_{21}^c\right)^2-\left(K_{31}^c\right)^2}}\right)\\
&\cdot\left(\left(y-\frac{d^c\cos\theta}{2}+\frac{D^c}{2}\right)(-\cos\theta)\right.\\
&\left.+\left(z-\frac{d^c\sin\theta}{2}\right)(-\sin\theta)\right),\\
\boldsymbol{S}_{1L_1} =& \left(\frac{K_{11}^c}{\sqrt{\left(K_{11}^c\right)^2+\left(K_{21}^c\right)^2-\left(K_{31}^c\right)^2}}-1\right)\\
&\cdot\left(-2\left(z-\frac{d^c\sin\theta}{2}\right)\right)\\
&+\left(\frac{K_{21}^c}{\sqrt{\left(K_{11}^c\right)^2+\left(K_{21}^c\right)^2-\left(K_{31}^c\right)^2}}\right)\\
&\cdot\left(-2\left(y-\frac{d^c\cos\theta}{2}+\frac{D^c}{2}\right)\right)\\
&+\left(\frac{-K_{31}^c}{\sqrt{\left(K_{11}^c\right)^2+\left(K_{21}^c\right)^2-\left(K_{31}^c\right)^2}}\right)\cdot 2L_1^c.
\end{aligned} \tag{71}$$

Similarly, Eq. (69) can be rewritten as

$$\sum_{r=1}^{4}\frac{\partial \boldsymbol{T}_1\left(\boldsymbol{K}_1\left(\boldsymbol{y^c}\right)\right)}{\partial \boldsymbol{K}_1\left(\boldsymbol{y^c}\right)}\cdot\frac{\partial \boldsymbol{K}_1\left(\boldsymbol{y^c}\right)}{\partial y_r}\Delta y_r = \boldsymbol{T}_{1D}\cdot\Delta D+\boldsymbol{T}_{1d}\cdot\Delta d+\boldsymbol{T}_{1L_1}\cdot\Delta L_1 \tag{72}$$

where

$$\begin{aligned}
\boldsymbol{T}_{1D} &= L_1^c+y-\frac{d^c\cos\theta}{2}+\frac{D^c}{2},\\
\boldsymbol{T}_{1d} &= -L_1^c\cos\theta+\left(y-\frac{d^c\cos\theta}{2}+\frac{D^c}{2}\right)(-\cos\theta)\\
&\quad+\left(z-\frac{d^c\sin\theta}{2}\right)(-\sin\theta),\\
\boldsymbol{T}_{1L_1} &= 2\left(y-\frac{d^c\cos\theta}{2}+\frac{D^c}{2}\right)+2L_1^c.
\end{aligned} \tag{73}$$

Substituting Eqs. (70) and (72) into (67), the interval radius $\Delta_1\boldsymbol{\gamma}_1$ of the interval luffing angular response vector can be rewritten as

$$\begin{aligned}
\Delta_1\boldsymbol{\gamma}_1 =& \left|\left[\left(\boldsymbol{T}_1^c\right)^{-1}\boldsymbol{S}_{1D}-\left(\boldsymbol{T}_1^c\right)^{-2}\boldsymbol{S}_1^c\boldsymbol{T}_{1D}\right]\cdot\Delta D\right.\\
&+\left[\left(\boldsymbol{T}_1^c\right)^{-1}\boldsymbol{S}_{1d}-\left(\boldsymbol{T}_1^c\right)^{-2}\boldsymbol{S}_1^c\boldsymbol{T}_{1d}\right]\cdot\Delta d\\
&\left.+\left[\left(\boldsymbol{T}_1^c\right)^{-1}\boldsymbol{S}_{1L_1}-\left(\boldsymbol{T}_1^c\right)^{-2}\boldsymbol{S}_1^c\boldsymbol{T}_{1L_1}\right]\cdot\Delta L_1\right|
\end{aligned} \tag{74}$$

Based on Eqs. (63) and (74), the upper bound $\overline{\boldsymbol{\gamma}_1}$ and lower bound $\underline{\boldsymbol{\gamma}_1}$ of the interval luffing angular response vector $\boldsymbol{\gamma}_1^I$ of the DACS with narrowly interval structure parameters calculated by FCFIPM can be expressed as

$$\overline{\boldsymbol{\gamma}_1}=\boldsymbol{\gamma}_1^c+\Delta_1\boldsymbol{\gamma}_1,\ \underline{\boldsymbol{\gamma}_1}=\boldsymbol{\gamma}_1^c-\Delta_1\boldsymbol{\gamma}_1. \tag{75}$$

Similarly, for the crane 2, the interval radius $\Delta_1\boldsymbol{\gamma}_2$ of the interval luffing angular response vector can be rewritten as

$$\begin{aligned}
\Delta_1\boldsymbol{\gamma}_2 =& \left|\left[\left(\boldsymbol{T}_2^c\right)^{-1}\boldsymbol{S}_{2D}-\left(\boldsymbol{T}_2^c\right)^{-2}\boldsymbol{S}_2^c\boldsymbol{T}_{2D}\right]\cdot\Delta D\right.\\
&+\left[\left(\boldsymbol{T}_2^c\right)^{-1}\boldsymbol{S}_{2d}-\left(\boldsymbol{T}_2^c\right)^{-2}\boldsymbol{S}_2^c\boldsymbol{T}_{2d}\right]\cdot\Delta d\\
&\left.+\left[\left(\boldsymbol{T}_2^c\right)^{-1}\boldsymbol{S}_{2L_2}-\left(\boldsymbol{T}_2^c\right)^{-2}\boldsymbol{S}_2^c\boldsymbol{T}_{2L_2}\right]\cdot\Delta L_2\right|
\end{aligned} \tag{76}$$

where

$$\boldsymbol{S}_{2D} = \left(\frac{K_{22}^c}{\sqrt{\left(K_{12}^c\right)^2 + \left(K_{22}^c\right)^2 - \left(K_{32}^c\right)^2}}\right) \cdot \left(L_2^c\right) + \left(\frac{-K_{32}^c}{\sqrt{\left(K_{12}^c\right)^2 + \left(K_{22}^c\right)^2 - \left(K_{32}^c\right)^2}}\right) \cdot (-1)\left(y + \frac{d^c \cos\theta}{2} - \frac{D^c}{2}\right),$$

$$\boldsymbol{S}_{2d} = \left(\frac{K_{12}^c}{\sqrt{\left(K_{12}^c\right)^2 + \left(K_{22}^c\right)^2 - \left(K_{32}^c\right)^2}} - 1\right) \cdot \left(-L_2^c \sin\theta\right) + \left(\frac{K_{22}^c}{\sqrt{\left(K_{12}^c\right)^2 + \left(K_{22}^c\right)^2 - \left(K_{32}^c\right)^2}}\right) \cdot \left(-L_2^c \cos\theta\right) + \left(\frac{-K_{32}^c}{\sqrt{\left(K_{12}^c\right)^2 + \left(K_{22}^c\right)^2 - \left(K_{32}^c\right)^2}}\right) \cdot \left(\left(y + \frac{d^c \cos\theta}{2} - \frac{D^c}{2}\right)(\cos\theta) + \left(z + \frac{d^c \sin\theta}{2}\right)(\sin\theta)\right),$$

$$\boldsymbol{S}_{2L_2} = \left(\frac{K_{12}^c}{\sqrt{\left(K_{12}^c\right)^2 + \left(K_{22}^c\right)^2 - \left(K_{32}^c\right)^2}} - 1\right) \cdot \left(-2\left(z + \frac{d^c \sin\theta}{2}\right)\right) + \left(\frac{K_{22}^c}{\sqrt{\left(K_{12}^c\right)^2 + \left(K_{22}^c\right)^2 - \left(K_{32}^c\right)^2}}\right) \cdot \left(-2\left(y + \frac{d^c \cos\theta}{2} - \frac{D^c}{2}\right)\right) + \left(\frac{-K_{32}^c}{\sqrt{\left(K_{12}^c\right)^2 + \left(K_{22}^c\right)^2 - \left(K_{32}^c\right)^2}}\right) \cdot 2L_2^c.$$

$$\boldsymbol{T}_{2D} = -L_2^c - y - \frac{d^c \cos\theta}{2} + \frac{D^c}{2},$$

$$\boldsymbol{T}_{2d} = L_2^c \cos\theta + \left(y + \frac{d^c \cos\theta}{2} - \frac{D^c}{2}\right)(\cos\theta) + \left(z + \frac{d^c \sin\theta}{2}\right)(\sin\theta),$$

$$\boldsymbol{T}_{2L_2} = 2\left(y + \frac{d^c \cos\theta}{2} - \frac{D^c}{2}\right) + 2L_2^c. \tag{77}$$

Similarly, the upper bound $\overline{\boldsymbol{\gamma}_2}$ and lower bound $\underline{\boldsymbol{\gamma}_2}$ of the interval luffing angular response vector $\boldsymbol{\gamma}_2^I$ of the DACS with narrowly interval structure parameters calculated by FCFIPM can be expressed as

$$\overline{\boldsymbol{\gamma}_2} = \boldsymbol{\gamma}_2^c + \Delta_1\boldsymbol{\gamma}_2, \underline{\boldsymbol{\gamma}_2} = \boldsymbol{\gamma}_2^c - \Delta_1\boldsymbol{\gamma}_2 \tag{78}$$

According to above analysis, we define the interval change ratios of interval variables are all varied in a same interval. If DD denotes the dispersal degree of uncertain variables of the ith crane of the DACS, then DD will vary in some interval.

To investigate the different effects of different interval parameters from interval models on the intervals of the luffing angular response field of the DACS, we take the interval model DD1 $= D_F = d_F = L_{1F} = L_{2F}$ as a reference, simulations obtained by the FCFIPM for the DACS response field problem are carried out by MATLAB R2014a on a 2.5 GHz Intel(R) Core (TM) i7–4710MQ CPU computer. The lower bound (LB) and upper bound (UB) of the luffing angular response of the crane 1 and crane 2 of the DACS calculated by the FCFIPM with different interval models are plotted in Figs. 17, 18, 19, 20 and Figs. 21, 22, 23 and 24, respectively.

Figures 17 and 21 depict the lower and upper bounds of the luffing angular response of the crane 1 and crane 2 calculated by the FCFIPM with/without D_F, respectively. In other words, where two interval models are taken as DD1 $= D_F = d_F = L_{1F} = L_{2F}$ and DD2 $= d_F = L_{1F} = L_{2F}, D_F = 0$. It is obvious that the change of D_F has impact on the lower and upper bounds of the luffing angular response of the crane 1 and crane 2, which means the length of A_1A_2 or D has significant impact on the intervals of the luffing angular response field of the DACS. Moreover, it is noted that both the intervals of the luffing angular response field of the crane 1 and crane 2 show decreasing trends when the interval parameter D is considered.

Figures 18 and 22 depict the lower and upper bounds of the luffing angular response of the crane 1 and crane 2 calculated by the FCFIPM with/without d_F, respectively. In other words, where two interval models are taken as DD1 $= D_F = d_F = L_{1F} = L_{2F}$ and DD2 $= D_F = L_{1F} = L_{2F}, d_F = 0$. It is obvious that the change of d_F has impact on the lower and upper

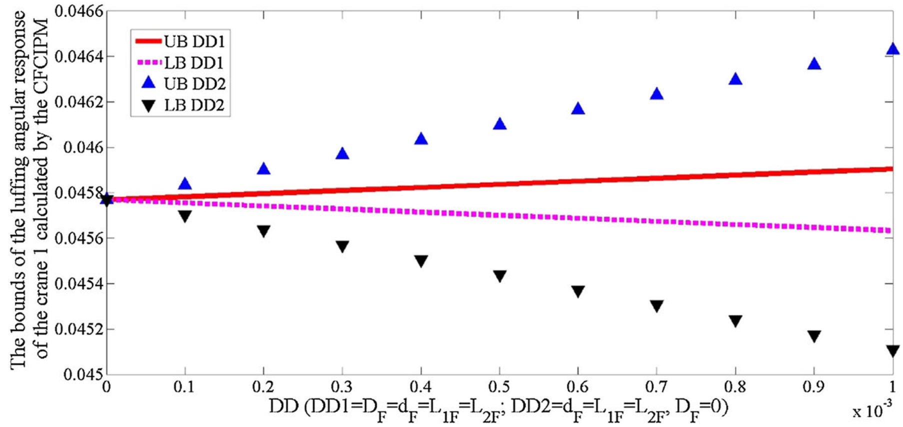

Fig. 17 The bounds of the luffing angular response of the crane 1 calculated by the FCFIPM with/without D_F

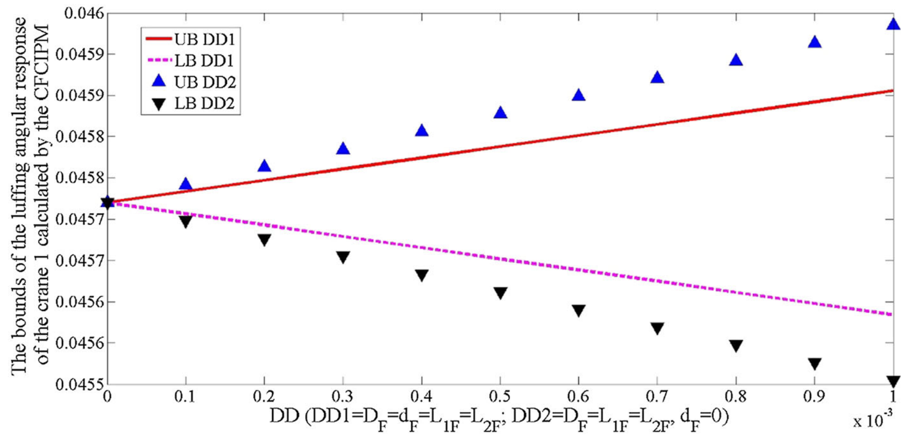

Fig. 18 The bounds of the luffing angular response of the crane 1 calculated by the FCFIPM with/without d_F

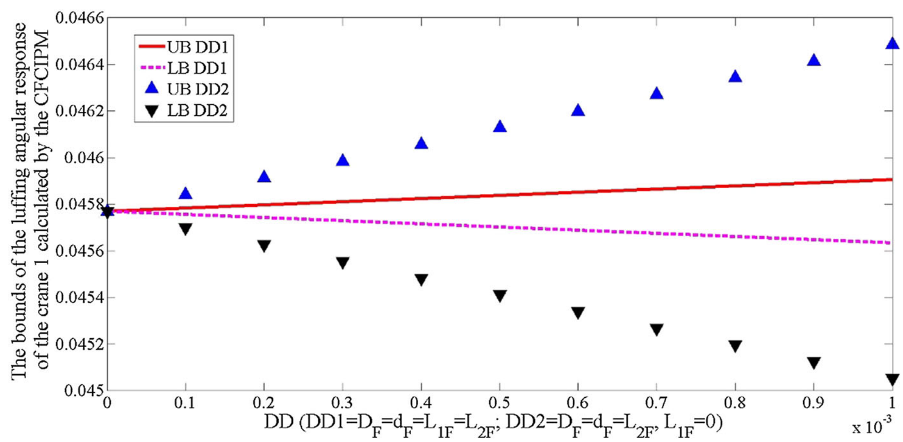

Fig. 19 The bounds of the luffing angular response of the crane 1 calculated by the FCFIPM with/without L_{1F}

bounds of the luffing angular response of the crane 1 and crane 2, which means the length of payload C_1C_2 or d has significant impact on the intervals of the luffing angular response field of the DACS. Moreover, it is noted that the interval of the luffing angular response field of the crane 1 shows a decreasing trend when the interval parameter d is considered; however, the interval of the luffing angular response field of the crane 2 shows an increasing trend when the interval parameter d is considered.

Figures 19 and 23 depict the lower and upper bounds of the luffing angular response of the crane 1 and crane

Fig. 20 The bounds of the luffing angular response of the crane 1 calculated by the FCFIPM with/without L_{2F}

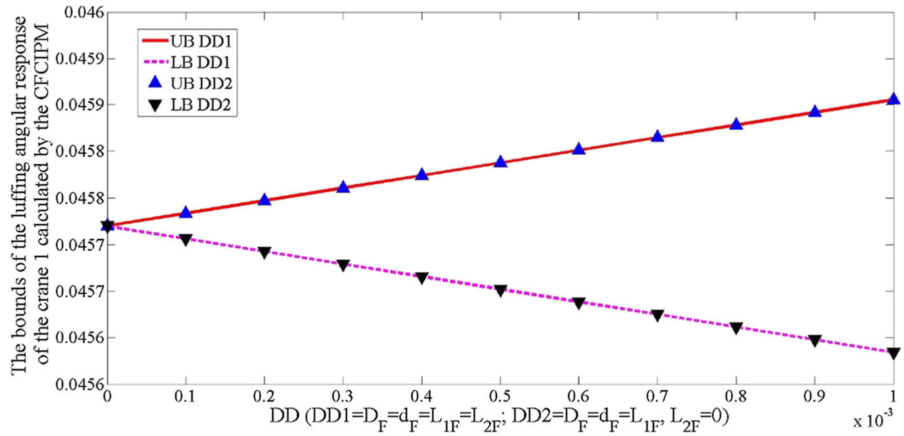

Fig. 21 The bounds of the luffing angular response of the crane 2 calculated by the FCFIPM with/without D_F

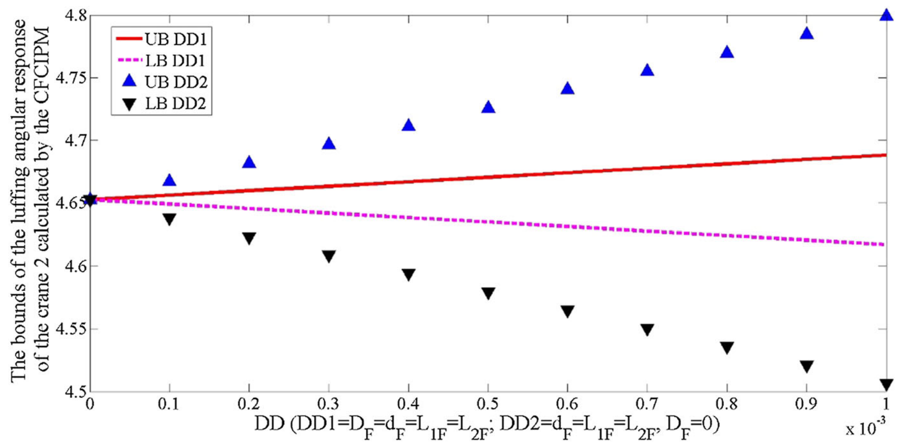

Fig. 22 The bounds of the luffing angular response of the crane 2 calculated by the FCFIPM with/without d_F

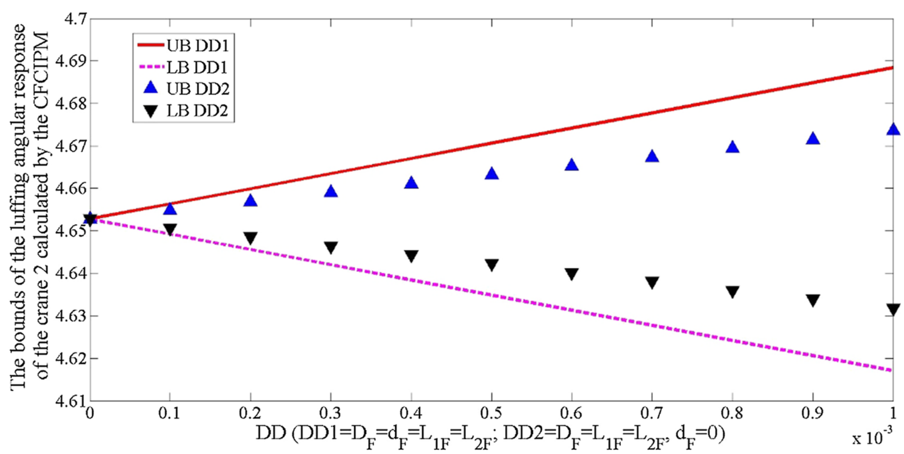

2 calculated by the FCFIPM with/without L_{1F}, respectively. In other words, where two interval models are taken as $\mathrm{DD1} = D_F = d_F = L_{1F} = L_{2F}$ and $\mathrm{DD2} = D_F = d_F = L_{2F}, L_{1F} = 0$. It is obvious that the change of L_{1F} has impact on the lower and upper bounds of the luffing angular response of the crane 1 but not those of the crane 2, which means the length of lifting arm A_1B_1 or L_1 has significant impact on the intervals of the luffing angular response field of the crane 1 but not the intervals of the luffing angular response field of the crane 2. Moreover, it is noted that the interval of the luffing angular response field of

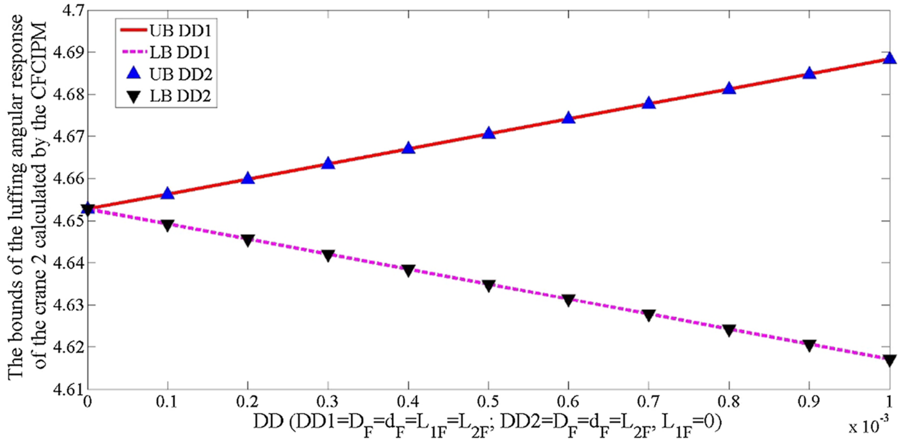

Fig. 23 The bounds of the luffing angular response of the crane 2 calculated by the FCFIPM with/without L_{1F}

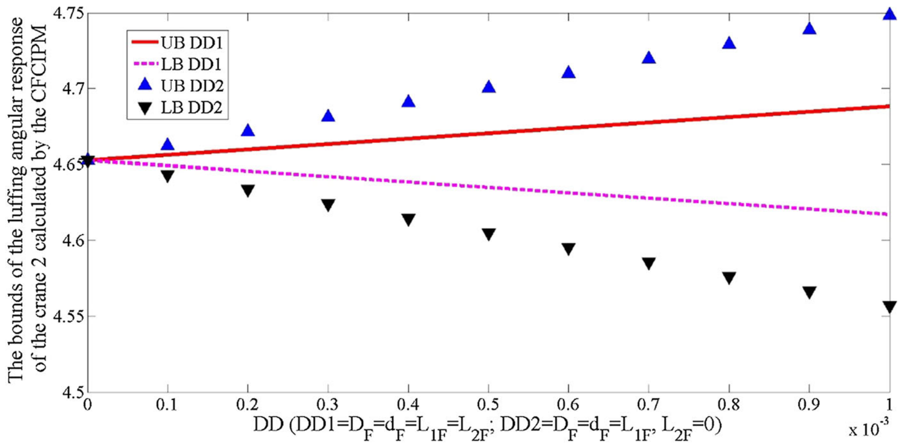

Fig. 24 The bounds of the luffing angular response of the crane 2 calculated by the FCFIPM with/without L_{2F}

the crane 1 shows an decreasing trend when the interval parameter L_1 is considered; however, the interval parameter L_1 does not have any impact on the interval of the luffing angular response field of the crane 2.

Figures 20 and 24 depict the lower and upper bounds of the luffing angular response of the crane 1 and crane 2 calculated by the FCFIPM with/without L_{2F}, respectively. In other words, where two interval models are taken as DD1 $= D_F = d_F = L_{1F} = L_{2F}$ and DD2 $= D_F = d_F = L_{1F}, L_{2F} = 0$. It is obvious that the change of L_{2F} has impact on the lower and upper bounds of the luffing angular response of the crane 2 but not those of the crane 1, which means the length of lifting arm A_2B_2 or L_2 has significant impact on the intervals of the luffing angular response field of the crane 2 but not the intervals of the luffing angular response field of the crane 1. Moreover, it is noted that the interval of the luffing angular response field of the crane 2 shows an decreasing trend when the interval parameter L_2 is considered; however, the interval parameter L_2 does not have any impact on the interval of the luffing angular response field of the crane 1.

Moreover, from Figs. 17, 18, 19 and 20, we can see that the length of lifting arm A_2B_2 does not have any impact on the lower and upper bounds of the luffing angular response of the crane 1, but the length of A_1A_2, the length of payload C_1C_2 and the length of lifting arm A_1B_1 have significant impact on the interval of the luffing angular response field of the crane 1, which means the main impact on the interval of the luffing angular response field of the crane 1 comes from interval parameters D, d, L_1.

From Figs. 21, 22, 23 and 24, we can see that the length of lifting arm A_1B_1 does not have any impact on the lower and upper bounds of the luffing angular response of the crane 2, but the length of A_1A_2, the length of payload C_1C_2 and the length of lifting arm A_2B_2 have significant impact on the interval of the luffing angular response field of the crane 2, which means the main impact on the interval of the luffing angular response field of the crane 2 comes from interval parameters D, d, L_2.

Furthermore, with the increase of the DD, the interval luffing angular response field increases accordingly, which means the DACS response field has the feature of interval variable due to the existence of interval parameters in the luffing angular response vectors of Eqs. (75) and (78).

Taken together, from Figs. 17, 18, 19 and 20, the results show the relative impact of factors on the luffing angular response field of the crane 1, from most significant to least significant: the length of lifting arm A_1B_1 (L_1), the length of A_1A_2 (D), the length of payload C_1C_2 (d). From Figs. 21, 22, 23 and 24, the results show the relative impact of factors on the luffing angular response field of the crane 2, from most significant to least significant: the length of A_1A_2 (D), the length of lifting arm A_2B_2 (L_2), the length of payload C_1C_2 (d).

To make the above results more clear, the impact of different interval parameters on the bounds of the luffing angular response of the crane 1 and crane 2 is listed in Table 4, respectively. Here, the symbol "+," "–" and "×" represent the trend of the increasing, decreasing and unchanging, respectively. We also take the interval model DD1 $= D_F = d_F = L_{1F} = L_{2F}$ as a reference.

To illustrate the accuracy and computational cost of FCFIPM for the luffing angular response field with interval parameters more clearly, we calculate the lower and upper bounds of the luffing angular response vector of the crane 1 and crane 2 of the DACS, the relative errors are also listed in Tables 5 and 6, respectively. Here, we also take the interval model DD $= D_F = d_F = L_{1F} = L_{2F}$ as research object. The results obtained by the Monte Carlo method are considered as referenced solutions, simulations of the MCM and FCFIPM for this interval luffing angular response field are also carried out by MATLAB R2014a on a 2.5 GHz Intel(R) Core (TM) i7–4710MQ CPU computer.

From Tables 5 and 6, when the DD is no more than 0.50%, we can see that the relative errors of the lower and upper bound of the luffing angular response vector of the crane 1 and crane 2 yielded by the FCFIPM are no more than 10%, which means the intervals of the luffing angular response of the crane 1 and crane 2 are close to those of the referenced values yielded

Table 4 The impact of interval parameters on the bounds of luffing angular response of the DACS

Interval of luffing angular response	Length of A_1A_2 (D)		Length of payload C_1C_2 (d)		Length of lifting arm A_1B_1 (L_1)		Length of lifting arm A_2B_2 (L_2)	
	DD1	DD2	DD1	DD2	DD1	DD2	DD1	DD2
Crane 1	Reference	–	Reference	–	Reference	–	Reference	×
Crane 2	Reference	–	Reference	+	Reference	×	Reference	–

Table 5 Bounds of the luffing angular response vector of the crane 1

DD $= D_F = d_F = L_{1F} = L_{2F}$	Bounds	MCM		FCFIPM		Error (%)
		Time (s)	Value	Time (s)	Value	
0.05%	LB	1.5625	0.0454	0.0071	0.0457	0.66
	UB		0.0461		0.0458	0.65
0.25%	LB	1.6459	0.0440	0.0077	0.0454	3.18
	UB		0.0475		0.0461	2.95
0.50%	LB	1.5865	0.0421	0.0072	0.0451	7.12
	UB		0.0491		0.0464	5.50
0.75%	LB	1.5982	0.0400	0.0069	0.0448	12.00
	UB		0.0457		0.0468	2.41
1.00%	LB	1.5838	0.0379	0.0061	0.0444	17.15
	UB		0.0521		0.0471	9.60

Table 6 Bounds of the luffing angular response vector of the crane 2

DD $=\Delta D_F=\Delta d_F=\Delta L_{1F}=\Delta L_{2F}$	Bounds	MCM		FCFIPM		Error (%)
		Time (s)	Value	Time (s)	Value	
0.05%	LB	1.5786	4.5571	0.0071	4.6349	1.71
	UB		4.5606		4.6705	2.35
0.25%	LB	1.6312	4.5498	0.0077	4.5987	1.07
	UB		4.5676		4.7417	3.81
0.50%	LB	1.8933	4.5413	0.0072	4.4747	1.47
	UB		4.5762		4.8307	5.56
0.75%	LB	1.5355	4.5321	0.0069	4.3857	3.23
	UB		4.5865		4.9197	7.26
1.00%	LB	2.0764	4.5237	0.0061	4.2967	5.02
	UB		4.5928		5.0087	9.06

by the MCM. In other words, the results calculated by the FCFIPM are completely acceptable if the DD of interval parameters is not high. When the DD starts to increase from 0.50% to 1.00%, the DACS response field produced by the FCFIPM significantly deviates from those yielded by the MCM, which indicates that the FCFIPM based on the differential property of composite function, the first-order Taylor series expansion and the Neumann series is more appropriate for the prediction of the DACS response field with narrowly interval parameters; in other words, the effects of neglecting the higher-order terms of Taylor series expansion and the higher-order terms of Neumann series in Eqs. (43), (46) and (50) are unpredictable and uncontrollable. Computational cost is another index to evaluate the performances of numerical methods, from the results listed in tables we can see that the FCFIPM is much more efficient and greatly reduce the executive time when compared with the MCM.

7 Conclusions

By combining interval perturbation method with composite function theory, this paper analyzes luffing angular response modeling and proposes a first-order composite function interval perturbation method (FCFIPM) to predict the luffing angular response field problem of the dual automobile cranes system (DACS) with narrowly interval structure parameters. The uncertainties in structure parameters are fully considered, which makes the equilibrium equation of luffing angular response vector of the DACS with interval parameters more objective. The uncertain interval structure parameters with certain lower and upper bounds are modeled as dynamics-based nonsingular interval model. In the FCFIPM, the luffing angular response vector expressions of crane 1 and crane 2 of the DACS are approximated based on the first-order Taylor series expansion and the Neumann series expansion. According to differential property of composite function and monotonic analysis technique, the lower and upper bounds of the interval luffing angular response vector of the crane 1 and crane 2 of the DACS are determined effectively.

Compared with MCM, numerical results on some interval DACS luffing angular response field examples verify the feasibility and efficiency of the FCFIPM when dealt with narrowly interval uncertainty. By treating uncertain structure parameters as narrowly interval variables, from the investigation of the different impacts of different interval parameters on the intervals of the luffing angular response field of the DACS, results show different effects of interval structure parameters (D, d, L_1, L_2) on the bounds of the interval luffing angular response vector of the crane 1 and crane 2 of the DACS. To be more specific, the relative impact of factors on the luffing angular response field of the crane 1, from most significant to least significant: the length of lifting arm A_1B_1 (L_1), the length of A_1A_2 (D), the length of payload C_1C_2 (d). The relative impact of factors on the luffing angular response field of the crane 2, from most significant to least significant: the length of A_1A_2 (D), the length of lifting arm A_2B_2 (L_2), the length of payload C_1C_2 (d).

From the investigation of the accuracy and computational cost of FCFIPM for the interval luffing angular response field, the FCFIPM is demonstrated to be much more superior than the MCM. However, it should be noted that the proposed method, based on the first-order Taylor series expansion and the first-order Neumann series expansion, is not suitable to DACS luffing angular response field problem with large ranges of interval variables or large uncertain levels of interval parameters. Although the accuracy of the proposed method can be improved by considering high-order Neumann series expansion, more computational efforts will be required. Thus, the first-order composite function interval perturbation method is a powerful tool for predicting interval luffing angular response field problem of the DACS with narrowly interval uncertainties.

Acknowledgements This work was supported by the National Natural Science Foundation of China (51575150 and 51605126).

References

1. Abdel-Rahman, E.M., Nayfeh, A.H., Masoud, Z.: Dynamics and control of cranes: a review. J. Vib. Control. **9**, 863–908 (2003)
2. Carmona, I.G., Collado, J.: Control of a two wired hammerhead tower crane. Nonlinear Dyn. **84**(4), 2137–2148 (2016)
3. Elbadawy, A.A., Shehata, M.M.G.: Anti-sway control of marine cranes under the disturbance of a parallel manipulator. Nonlinear Dyn. **82**(1), 1–20 (2015)
4. Sağirli, A., Boğoçlu, M.E., Ömürlü, V.E.: Modeling the dynamics and kinematics of a telescopic rotary crane by the bond graph method: part i. Nonlinear Dyn. **33**(33), 353–367 (2003)
5. Uchiyama, N.: Robust control of rotary crane by partial-state feedback with integrator. Mechatronics **19**(8), 1294–1302 (2009)
6. Zhang, M., Ma, X., Chai, H., Rong, X., Tian, X., Li, Y.: A novel online motion planning method for double-pendulum overhead cranes. Nonlinear Dyn. **85**(2), 1079–1090 (2016)
7. Fang, Y., Wang, P., Sun, N., Zhang, Y.: Dynamics analysis and nonlinear control of an offshore boom crane. IEEE Trans. Ind. Electron. **61**(1), 414–427 (2014)
8. Leban, F.A., Diaz-Gonzalez, J., Parker, G.G., Zhao, W.: Inverse kinematic control of a dual crane system experiencing base motion. IEEE Trans. Control Syst. Technol. **23**, 331–339 (2015)
9. Zi, B., Sun, H., Zhang, Dan: Design, analysis and control of a winding hybrid-driven cable parallel manipulator. Robot. Comput. Integr. Manuf. **48**, 196–208 (2017)
10. Qian, S., Zi, B., Ding, H.F.: Dynamics and trajectory tracking control of cooperative multiple mobile cranes. Nonlinear Dyn. **83**, 89–108 (2016)
11. Qian, S., Zi, B., Zhang, D., Zhang, L.: Kinematics and error analysis of cooperative cable parallel manipulators for multiple mobile cranes. Int. J. Mech. Mater. Des. **10**(4), 395–409 (2014)
12. Sun, N., Fang, Y., Chen, H., Lu, B.: Slew/translation positioning and swing suppression for 4-DOF tower cranes with parametric uncertainties: design and hardware experimentation. IEEE Trans. Ind. Electron. **63**, 6407–6418 (2016)
13. Sun, N., Fang, Y., Chen, H.: Adaptive antiswing control for cranes in the presence of rail length constraints and uncertainties. Nonlinear Dyn. **81**(1–2), 41–51 (2015)
14. Impollonia, N., Muscolino, G.: Interval analysis of structures with uncertain-but-bounded axial stiffness. Comput. Methods. Appl. Mech. Eng. **200**, 1945–1962 (2011)
15. Gao, W., Song, C.M., Tin-Loi, F.: Probabilistic interval analysis for structures with uncertainty. Struct. Saf. **32**, 191–199 (2010)
16. Shinozuka, M., Astill, C.J.: Random eigenvalue problems in structural analysis. AIAA J. **10**(10), 456–462 (2015)
17. Wang, C., Qiu, Z., Yang, Y.: Uncertainty propagation of heat conduction problem with multiple random inputs. Int. J. Heat Mass Transf. **99**, 95–101 (2016)
18. Wang, C., Qiu, Z.: Hybrid uncertain analysis for steady-state heat conduction with random and interval parameters. Int. J. Heat Mass Transf. **80**, 319–328 (2015)
19. Wang, C., Qiu, Z.: Subinterval perturbation methods for uncertain temperature field prediction with large fuzzy parameters. Int. J. Therm. Sci. **100**, 381–390 (2015)
20. Wang, M., Huang, Q.: A new hybrid uncertain analysis method for structural-acoustic systems with random and interval parameters. Comput. Struct. **175**, 15–28 (2016)
21. Xia, B., Yu, D.: Response probability analysis of random acoustic field based on perturbation stochastic method and change-of-variable technique. J. Vib. Acoust. **135**(5), 521–523 (2013)
22. Yin, S., Yu, D., Yin, H., Xia, B.: A unified method for the response analysis of interval/random variable models of acoustic fields with uncertain-but-bounded parameters. Int. J. Numer. Methods. Eng. **111**(6), 503–528 (2017)
23. Xia, B., Yu, D., Han, X.: Unified response probability distribution analysis of two hybrid uncertain acoustic fields. Comput. Methods. Appl. Mech. Eng. **276**(7), 20–34 (2014)
24. Bai, Y.C., Jiang, C., Han, X., Hu, D.A.: Evidence-theory-based structural static and dynamic response analysis under epistemic uncertainties. Finite. Elem. Anal. Des. **68**(3), 52–62 (2013)
25. Jiang, C., Ni, B.Y., Han, X.: Non-probabilistic convex model process: a new method of time-variant uncertainty analysis and its application to structural dynamic reliability problems. Comput. Methods Appl. Mech. Eng. **268**(1), 656–676 (2014)
26. Zi, B., Zhou, B.: A modified hybrid uncertain analysis method for dynamic response field of the LSOAAC with random and interval parameters. J. Sound. Vib. **374**, 111–137 (2016)
27. Do, D., Gao, W., Song, C.: Dynamic analysis and reliability assessment of structures with uncertain-but-bounded parameters under stochastic process excitations. Reliab. Eng. Syst. Saf. **132**, 46–59 (2014)
28. Pietro, T., Seymour, M., Luigi, P., Pirrotta, A., Kareem, A.: An efficient framework for the elasto-plastic reliability assessment of uncertain wind excited systems. Struct. Saf. **58**, 69–78 (2016)

29. Wu, B., Wu, D., Gao, W.: Time-variant random interval response of concrete-filled steel tubular composite curved structures. Compos. Part B Eng. **94**, 122–138 (2016)
30. Wu, D., Gao, W., Feng, J.: Structural behaviour evolution of composite steel-concrete curved structure with uncertain creep and shrinkage effects. Compos. Part B Eng. **86**, 261–272 (2015)
31. Zi, B., Zhou, B., Qian, S.: Dynamic modeling and analysis of cable parallel manipulator for dual automobile cranes during luffing motion. J. Mech. Eng. doi:10.3901/JME.2016.06.198 **(in Chinese)**
32. Neumaier, A.: Interval Methods for Systems of Equations. Cambridge University Press, Cambridge (1990)
33. Armiyoon, A.R., Wu, C.Q.: A novel method to identify boundaries of basins of attraction in a dynamical system using Lyapunov exponents and Monte Carlo techniques. Nonlinear Dyn. **79**(1), 275–293 (2014)
34. Chen, N., Yu, D., Xia, B.: Hybrid uncertain analysis for the prediction of exterior acoustic field with interval and random parameters. Comput. Struct. **141**, 9–18 (2014)
35. Xia, B., Yu, D., Liu, J.: Hybrid uncertain analysis of acoustic field with interval random parameters. Comput. Method. Appl. Mech. Eng. **256**(4), 56–69 (2013)
36. Wang, C., Qiu, Z.: An interval perturbation method for exterior acoustic field prediction with uncertain-but-bounded parameters. J. Fluids Struct. **49**, 441–449 (2014)
37. Wang, C., Qiu, Z.: Interval analysis of steady-state heat convection-diffusion problem with uncertain-but-bounded parameters. Int. J. Heat Mass Transf. **91**, 355–362 (2015)
38. Xia, B., Yu, D.: Modified interval perturbation finite element method for a structural-acoustic system with interval parameters. J. Appl. Mech. **80**(4), 041027 (2013)
39. Xia, B., Yu, D., Liu, J.: Interval and subinterval perturbation methods for a structural-acoustic system with interval parameters. J. Fluids Struct. **38**(3), 146–163 (2013)
40. Muscolino, G., Santoro, R., Sofi, A.: Explicit sensitivities of the response of discretized structures under stationary random processes. Probabilist. Eng. Mech. **35**(1), 82–95 (2014)
41. Sofi, A., Muscolino, G.: Static analysis of Euler–Bernoulli beams with interval Young's modulus. Comput. Struct. **156**, 72–82 (2015)
42. Muscolino, G., Santoro, R., Sofi, A.: Explicit frequency response functions of discretized structures with uncertain parameters. Comput. Struct. **133**, 64–78 (2014)
43. Muscolino, G., Sofi, A.: Bounds for the stationary stochastic response of truss structures with uncertain-but-bounded parameters. Mech. Syst. Signal Process. **37**(37), 163–181 (2013)
44. Wu, J., Zhang, Y., Chen, L., Luo, Z.: A Chebyshev interval method for nonlinear dynamic systems under uncertainty. Appl. Math. Model. **37**(6), 4578–4591 (2013)
45. Wang, Z., Tian, Q., Hu, H.: Dynamics of spatial rigid-flexible multibody systems with uncertain interval parameters. Nonlinear Dyn. **84**(2), 527–548 (2016)
46. Qian, S., Zi, B., Ding, H.F., Kecskemethy, A.: Design and analysis of cooperative cable parallel manipulators for multiple mobile cranes. Int. J. Adv. Robot. Syst. **9**, 1–9 (2012)
47. Zhu, Z., Dou, R.: Optimum design of 2-DOF parallel manipulators with actuation redundancy. Mechatronics **19**, 761–766 (2009)
48. Wu, J., Wang, J., You, Z.: A comparison study on the dynamics of planar 3-DOF4-RRR, 3-RRRand 2-RRR parallel manipulators. Robot. Comput. Integr. Manuf. **27**, 150–156 (2011)
49. Jiang, C., Ni, B., Liu, N.: Interval process model and non-random vibration analysis. J. Sound. Vib. **373**, 104–131 (2016)
50. Kim, J.: Delay-dependent robust H_∞ filtering for uncertain discrete-time singular systems with interval time-varying delay. Automatica **46**(3), 591–597 (2010)